Modification of the Deep Salinity-Maximum in the Southern Ocean by Circulation in the Antarctic Circumpolar Current and the Weddell Gyre

Matthew Donnelly[1], Harry Leach[2] and Volker Strass[3]

[1]British Oceanographic Data Centre, National Oceanography Centre, Joseph Proudman Building, 6 Brownlow Street, Liverpool, L3 5DA, UK

[2]Department of Earth, Ocean and Ecological Sciences, University of Liverpool, 4 Brownlow Street, Liverpool, L69 3GP, UK

[3]Alfred-Wegener-Institut Helmholtz-Zentrum für Polar- und Meeresforschung, Postfach 12 01 61, D-27515 Bremerhaven, Germany

Corresponding author: Matthew Donnelly
E-mail: matdon@bodc.ac.uk
Telephone: +44 151 795 4892

Abstract

The evolution of the deep salinity-maximum associated with the Lower Circumpolar Deep Water (LCDW) is assessed using a set of 37 hydrographic sections collected over a 20 year period in the Southern Ocean as part of the WOCE/CLIVAR programme. A circumpolar decrease in the value of the salinity maximum is observed eastwards from the North Atlantic Deep Water (NADW) in the Atlantic sector of the Southern Ocean through the Indian and Pacific sectors to Drake Passage. Isopycnal mixing processes are limited by circumpolar fronts, and in the Atlantic sector this acts to limit the direct poleward propagation of the salinity signal. Limited entrainment occurs into the Weddell Gyre, with LCDW entering primarily through the eddy-dominated eastern limb. A vertical mixing coefficient, κ_V of (2.86 ± 1.06) x 10^{-4} m^2 s^{-1} and an isopycnal mixing coefficient, κ_I of (8.97 ± 1.67) x 10^2 m^2 s^{-1} are calculated for the eastern Indian and Pacific sectors of the Antarctic Circumpolar Current (ACC). A κ_V of (2.39 ± 2.83) x 10^{-5} m^2 s^{-1}, an order of magnitude smaller, and a κ_I of (2.47 ± 0.63) x 10^2 m^2 s^{-1}, three times smaller, are calculated for the southern and eastern Weddell Gyre reflecting a more turbulent regime in the ACC and a less turbulent regime in the Weddell Gyre. In agreement with other studies, we conclude that the ACC acts as a barrier to direct meridional transport and mixing in the Atlantic sector evidenced by the eastward propagation of the deep salinity-maximum signal, insulating the Weddell Gyre from short-term changes in NADW characteristics.

Keywords: Southern Ocean; Antarctic Circumpolar Current; Weddell Gyre; Warm Deep Water; Lower Circumpolar Deep Water; North Atlantic Deep Water; deep salinity maximum; entrainment; mixing.

1 - Introduction

The Southern Ocean is dominated by two main circulation features: the Antarctic Circumpolar Current (ACC) and the Meridional Overturning Circulation (MOC). The MOC acts on a global scale to transport North Atlantic Deep Water (NADW) southwards into the Southern Ocean, where it is modified to form Circumpolar Deep Water (CDW) by exchanges with the other ocean basins during its circulation around Antarctica with the ACC. CDW is brought towards the surface along sloping isopycnals by wind-driven upwelling in the Antarctic Divergence. The lighter fraction of the CDW returns back northwards with the upper branch of the MOC, and after undergoing further modification makes a major contribution to the Antarctic Intermediate Water (AAIW) which subducts in the Antarctic Convergence. A denser CDW fraction, including Lower Circumpolar Deep Water (LCDW) identified by a deep salinity maximum derived from the NADW (Patterson and Whitworth 1990), is advected farther southwards along trajectories which are further complicated by the presence of Antarctic gyres (Orsi et al. 1993; Fahrbach et al. 1994, 1995). Within these gyres modified local forms of LCDW, such as the fresher Warm Deep Water (WDW) in the Weddell Gyre, undergo further changes driven by sea-ice formation over the continental shelf and interactions with the ice shelves that lead to the formation of Weddell Sea Deep and Bottom Waters (WSDW and WSBW). Mixing of WSDW and LCDW (Speer and Zenk (1993), Zenk and Hogg (1996), Rhein et al. (1998), Stramma and England (1999), Vanicek and Siedler (2002)) eventually forms the Antarctic Bottom Water (AABW) which spreads northwards to fill most of the deep basins of the world ocean (Purkey and Johnson, 2010). Transformation of the LCDW in the Southern Ocean is therefore intimately linked to closing the lower limb of the global overturning circulation between the high northern and high southern latitudes (Marshall and Speer 2012).

Simultaneously and superimposed on the MOC, the eastward flowing ACC is a sustained circumpolar flow within which Antarctic Surface Water (AASW), AAIW, CDW and AABW are transported. These water masses are often treated as being relatively homogeneous due to their circumpolar distribution, however local variations in properties have been demonstrated to exist owing to variable rates and characteristics of water mass modification processes.

The transport of the ACC is associated with circumpolar fronts formed by strong meridional density gradients. The common major fronts from north to south (see Figure 1) are: the Sub-Antarctic Front (SAF), Polar Front (PF), the Southern ACC Front (SACCF) and the Southern Boundary (SB). North of the SAF lies the Sub-Antarctic Zone (SAZ), which in terms of water masses is dominated at depth by the NADW in the

Atlantic sector of the Southern Ocean. The ACC includes the enhanced transport associated with the SAF, PF and SACCF and incorporates the Polar Front Zone (PFZ) between the SAF and the PF and Antarctic Zone (AZ) to the south of the PF, dominated at depth by the CDW. South of the SB of the ACC lie the coastal waters and Antarctic gyres dominated by local deep water masses modified from CDW (Orsi et al. 1995). These represent clear circulation regimes.

A more refined view, presented by Sokolov and Rintoul (2009a, 2009b), identifies the consistent alignment of multiple ACC jets/frontal filaments with particular dynamic height contours along the circumpolar path; they show that the positions of these fronts vary but are consistently present, which in turn supports a quasi-constant transport for the ACC. This work suggests that the circulation of water masses several times around the Antarctic within the ACC, which exhibits a stable volume transport in the long-term despite short-term variability provided by mesoscale eddies, may provide the conditions for dampening temporal variability in the LCDW. Mixing by the eddies causes a downstream change in the salinity-maximum of the LCDW as it is advected around the Southern Ocean.

Many studies have sought to examine either one or the other circulation feature. However, it is their combined spatial and temporal variability acting upon hydrographic properties which together give rise to the distribution of conservative tracers. This is well demonstrated by the distribution of salinity along the Neutral Density surface, γ_n = 28.05 kg m^{-3} shown in Figure 1. This Neutral Density surface corresponds to the density of the spatially variable core of the deep salinity-maximum. The highest values are found in the South Atlantic, with an eastward extending core evident through the Indian and Pacific sectors of the Southern Ocean. In Drake Passage the LCDW salinity maximum has been observed as reaching a local practical salinity minimum of S_P ~34.73 by Whitworth and Nowlin (1987) and Naveira Garabato et al. (2002). Upon return to the South Atlantic there is a strong meridional salinity gradient across the ACC spanning a depth range of approximately 2000 m, with the most saline waters found at depths of ~2500m to the north and the freshest deep waters at depths of ~500m found in the gyre to the south. Meanders in the surface fronts of the ACC are co-located with meanders in the contours of salinity maxima.

Variability of the transport in the Southern Ocean and the characteristics of CDW over different timescales have been noted by a variety of authors. Gille (2002) reports on a long term warming by comparing Argo float data with earlier hydrographic data. Meredith and Hogg (2006) used satellite altimeter data and numerical modelling to investigate how eddy kinetic energy was increased following an increase in the mean zonal winds with a delay of a few years. Sokolov and Rintoul (2009a, 2009b) stress the long term stability of the structure of the ACC despite short term and regional variability. Turner and Overland (2009) compare and contrast recent climate trends in both polar regions: while the Arctic has been characterised by reducing sea ice cover this has not been the case in the Antarctic. Here the Peninsula has warmed due to changing winds and ice shelves have been subject to enhanced melting due to the intrusion of Deep Water onto the shelves. Indeed many authors have investigated regional processes involving the LCDW in particular sectors of the Southern Ocean (for example: Naveira Garabato et al. (2002) in the Scotia Sea, Gladyshev (2008) along 30^{o}E, and Bindoff et al. (2000, 2009) in the Ross Sea). Callahan (1972) examines the general distribution of water masses across the deep Southern Ocean, identifying the broad trends in the LCDW: the LCDW originates from the NADW and moves south from the South Atlantic and southwest Indian Ocean, with the distribution of LCDW determined predominantly by zonal advection, whilst vertical advection and mixing are relatively weak. Williams et al. (2006) provide a detailed study of the variability of the LCDW within Drake Passage and observe no long-term trend in the salinity-maximum between 1926 and 2004. They also provide a brief examination of the circumpolar characteristics of the LCDW, recognising a freshening and cooling of the NADW signal eastwards from the South Atlantic through to Drake Passage, but do not examine the Atlantic sector itself. However, a detailed recent examination of the circumpolar change of the salinity maximum along the ACC seems absent since Callahan (1972).

A crucial role in the interaction between the ACC and the MOC, and in the balancing of the movement of water masses, is taken by mixing. It is recognised that at different spatial and temporal scales different mechanisms for mixing can be less or more important, with the size of vertical and horizontal mixing being scale dependent (Okubo 1971, Ledwell et al. 1998). For instance, mesoscale stirring brings waters of different properties into closer proximity, so that interleavings, overturnings, double diffusion and finally molecular diffusion can contribute to the evolution of local water mass properties. In the spirit of Munk (1966), on a global scale the bulk mixing between different water masses – irrespective of exactly how that mixing occurs – forms an important and intrinsic part of the global thermohaline circulation.

There have been many studies of mixing conducted in a variety of ocean regimes which have produced a variety of estimates for mixing in different ocean regimes. It is important to contrast this range of mixing estimates to provide context for testing the hypothesis that the more quiescent Weddell Gyre and the more turbulent ACC have significantly different rates of mixing due to the different topographic and hydrographic conditions, despite both being elements of the Southern Ocean circulation. One of the earliest estimates of mixing was made by Munk, who, considering the horizontal mixing coefficient, κ_H, required a value of 5 x 10^3 m^2 s^{-1} in order to obtain a realistic scale for the western boundary current of a wind driven gyre in an analytical calculation (Munk 1950). Munk (1966) estimates a bulk vertical mixing coefficient, κ_V of 1.3 x 10^{-4} m^2 s^{-1} for the Pacific interior using a vertical advective-diffusive balance for a variety of parameters. In the Brazil Basin Polzin et al. (1997), using both turbulence measurements and tracers, demonstrate the spatial variability of mixing in the abyssal ocean, with κ_D = 0.1 x 10^{-4} m^2 s^{-1} over smooth topography, and a higher value of 5 x 10^{-4} m^2 s^{-1} within 150 m of the sea floor and over rougher topography. A more recent study by Ledwell et al. (2010), again using turbulence measurements and tracers, diagnosed a diapycnal mixing coefficient, κ_D = (1.3 ± 0.2) x 10^{-5} m^2 s^{-1} in the eastern Pacific sector of the ACC averaged over 1 year and thousands of kilometres. Naveira Garabato et al. (2004a) using in situ measurements obtained a range of values for the vertical mixing coefficient, κ_V, of 3 x 10^{-4} m^2 s^{-1} to 1 x 10^{-2} m^2 s^{-1} in weakly stratified Nordic Seas with the largest values relating to tidal activity near rough topography. Cisewski et al. (2005, 2008) obtain a κ_V of 7 x 10^{-4} m^2 s^{-1} in the upper pycnocline of the ACC at about 20ºE based on in situ turbulence measurements. Hibbert et al. (2009) diagnosed a maximum κ_V of 3 x 10^{-4} m^2 s^{-1} and κ_H of 30-100 m^2 s^{-1} within a cold core eddy of the ACC by looking at the heat budget of the Winter Water. Leach et al. (2011) looked at the modification of the WDW core as it flows westwards and found the Weddell Gyre to be relatively quiescent with κ_V of only 3 x 10^{-6} m^2 s^{-1}, one of the lowest values reported anywhere, and κ_H of 70-140 m^2 s^{-1}. Lenn et al. (2009) found a similarly quiescent regime in the Arctic, which is an interesting hydrographic regime to compare with the Weddell Gyre: both are areas of seasonal sea-ice cover with a mid-depth intrusion of relatively warm water. Sheen et al. (2013) report values for κ_V ranging from 10^{-5} m^2 s^{-1} at mid-depth to 10^{-3} m^2 s^{-1} near the bottom in the Scotia Sea based on in situ measurements and Waterman et al. (2013) have similar results near Kerguelen. These provide a useful backdrop for this study. As will be addressed in the methods section of this paper, there are different approaches and definitions when determining mixing through the water column. For purposes of inter-study comparison, the vertical mixing coefficient (κ_V) and diapycnic mixing coefficient (κ_D), along with the horizontal mixing coefficient (κ_H) and isopycnic mixing coefficient (κ_I), can be considered to be roughly analogous, however they are derived by different means within different frameworks and this must be remembered whilst comparing values. In the centres of ocean gyres, where isopycnals do not significantly slope, the difference between the two sets of quantities is less than in the ACC where the isopycnals associated with the ACC fronts are inclined to the isobars.

The objectives of the work presented in this paper are to examine the temporal and spatial variability of the deep salinity maximum associated with LCDW, assess how this salinity signal is propagated and to calculate bulk estimates of the horizontal and vertical diffusion in the Southern Ocean. To this end the WOCE/CLIVAR (http://cchdo.ucsd.edu/) CTD data set has been used. This represents a high quality homogeneous primary data set, though it is not as uniform in space and time as might be desired, but is not subject to any assumptions about the circulation or mixing in the Southern Ocean. To calculate the diffusion coefficients a relatively simple advective-diffusive balance has been assumed.

2 - Data

This study has made use of the available 'merged'-format Conductivity Temperature and Depth (CTD) sonde data from the CLIVAR and Carbon Hydrographic Data Office (CCHDO) website (http://whpo.ucsd.edu/). The CCHDO website provided a readily searchable range of international data which was openly available for use and gave access to a circumpolar coverage of hydrographic data. An earlier study examining the LCDW by Williams et al. (2006) primarily focused on Drake Passage, although used a similar but less extensive set of sections to complete a cursory review of the circumpolar salinity changes. They likewise obtained their circumpolar data from the CCHDO, however this study makes use of additional cruise data which has more recently been released through the CCHDO.

In total 37 hydrographic sections were used in this study, as detailed in Table 1. The earliest cruise undertaken was the SR02-A section along the Greenwich Meridian in 1989, and the latest was the I06S section undertaken in 2008 along 30ºE. Only those stations falling on the main section of each cruise were used, and only those stations whose profile reached an observable salinity maximum peak associated with the core of LCDW were considered for analysis.

A further section, P17A in the Pacific sector undertaken in 1992 by the RV Knorr was not included in this study due to a large longitudinal shift in the middle of the cruise track. This shift in cruise track was covered by only a single station spanning the vicinity of the Udintsev and Eltanin Fracture Zones (see Figure 2) on an orientation nearly perpendicular to the known topographically steered ACC path in that area (Orsi et al. 1995). As such it was deemed unwise for inclusion in the analysis as any re-gridding of data would introduce unacceptable levels of uncertainty.

Two further sections, P17E (1992) by the RV Knorr and P18 (1994) by the NOAAS Discoverer in the Pacific sector, were excluded as the cruises did not extend sufficiently far south to reach the Southern Boundary of the ACC, likely due to ice cover during the time of occupation. The Ross Gyre in general is poorly sampled compared with the rest of the Southern Ocean, and as a result it has not been possible to include its impacts on the LCDW within this study.

The approximate position of the Polar Front, as defined by Orsi et al. (1995), was used as a proxy for the centre of the mean ACC path in order to obtain a circumpolar trajectory, as shown in Figure 3.

Finally, estimates of ocean velocity were obtained from the Estimating the Circulation & Climate of the Ocean (ECCO) project. This data was obtained from the Live Access Server for ECCO-GODAE version 3, iteration 73 using the adjoint method, with 1 degree horizontal resolution and 23 vertical levels. The model solutions span 1992-2007 which includes the majority of the timeframe of the CCHDO data and was the most suitable of the available solutions for this study.

3 - Temporal and Spatial Variability of the Salinity-Maximum

3.1 - Methods – Identifying the Salinity-Maximum and Delineating Sub-sections

The initial step in examining the variability of the NADW north of the ACC, the LCDW within the ACC and the WDW in the Weddell Gyre is to evaluate the distribution of the salinity signal in space and time. This includes examining individual cruise potential temperature-practical salinity (θ-S_P) plots and comparing conservative temperature and absolute salinity (Θ-S_A) plots for the salinity-maximum across all cruises.

In order to examine the circumpolar spatial variability of the salinity-maximum associated with the LCDW it is necessary to consider the different regimes in which it is present. Firstly, it is necessary to separate NADW in the South Atlantic Gyre from the LCDW in the ACC, and the LCDW in the ACC from the WDW in the Weddell Gyre. This was achieved through setting maximum (1.823 dyn m) and minimum (0.732 dyn m) limits for the dynamic height at 20 m referenced to 2500 m as a proxy for the respective northern and southern boundary of the ACC, as observed in the data for Drake Passage. A depth of 20 m provides a consistent level at which all stations were sampled to avoid problems with missing data from the near-surface of profiles. Williams et al. (2006) use a reference level of 2000 m for their investigation of LCDW variability, however Sokolov and Rintoul (2009a) use a deeper reference level of 2500m which maximises the mass included in the dynamic height calculation whilst minimising the area of ocean discounted due to shallower topography, and the latter was deemed the preferable reference level.

The next step is to partition the Atlantic Sector of the ACC into the Polar Front Zone and the Antarctic Zone by establishing a section specific position for the Polar Front. There are many different definitions based on different parameters at different depths. In this study the 2.2ºC isotherm at 800m (Orsi et al. 1995) was chosen as the preferable option as it is a deep, as opposed to surface signature, which was clearly observable in almost all sections.

The final step in section partitioning was to delineate between the northern and southern limbs of the Weddell Gyre. After interrogation of the data, the criterion used to determine the central axis of the Weddell Gyre for each individual occupation of a section was the latitude of maximum Neutral Density at 300 m, which coincides approximately with the depth of the Salinity-maximum in the WDW. This doming of density surfaces is thought to be related to variability in the transport of the Weddell Gyre (Meredith et al. 2011), with the northward/southward sloping of the surfaces related to eastward/westward transport of the cyclonic circulation. Thus the maximum in Neutral Density represents an estimate of the central axis where near zero-flow occurs, and this was seen to vary in latitude from cruise to cruise.

Using this partitioning, an examination of the variability along the circumpolar path of the LCDW can be conducted with respect to longitude and time, taking into consideration depth and the value of the salinity-maximum.

3.2 - Methods - Appropriateness of Sampling

The majority of cruise sections used in this study (Figure 3) have been undertaken with a regular sampling pattern where a standard distance exists between one station and the next, within the limits of a research vessel being able to maintain station. Given that small scale fluctuations over these distances are at least as large as the variability between stations; this negated the need to grid the CTD data onto an equidistant spacing. Such a gridding process would introduce unnecessary error and false confidence in data coverage. Furthermore, the partitioning of sections in the Atlantic Sector of the Southern Ocean into their various regimes avoids the likelihood of cross-regime sampling bias.

The only region where station spacing is cause for concern is the varying northern coverage of the South Atlantic. However, as this study only refers to this northerly data generically as a source of the LCDW signal, and is not involved in subsequent mixing calculations there was no need to attempt to regularise the data distribution. Given the generally sparse and irregular sampling of more northerly waters in this dataset, it would be even less desirable to attempt to re-grid this northerly data than in the case of the more regularly spaced data straddling the ACC and Weddell Gyre.

3.3 - Methods - ACC and Weddell Gyre Track Length

The along ACC path distance was calculated between each pair of sections using the position of the Polar Front estimated by Orsi et al. (1995). The Polar Front roughly corresponds to the latitudinal centre of the ACC, however frontal positions can vary in time by up to 5º latitude as described by Moore et al. (1999). In addition, branches of the main fronts diverge and converge at various points in time and space around the Southern Ocean, as described by Sokolov and Rintoul (2009a, 2009b). Therefore, any representation of the fronts will at best be an approximation to the mean state and therefore the position of the Polar Front from Orsi et al. (1995) is considered a sufficient approximation to the mean ACC path length. This was used for both demonstrating spatial variability and for calculating a term of the mixing equation.

In order to determine an estimate of the pathway of the LCDW/WDW through the Weddell Gyre, the partitioned sections were analysed to identify an approximate latitudinal centre for each section. In conjunction with examining the circumpolar salinity trend, a corresponding distance track was calculated using Ocean Data View's 'Graphic Objects' tool which enabled the plotting of an estimated circulation pathway and calculation of its length.

3.4 - Results - Regional Variability of the Salinity-Maximum

The salinity-maximum associated with the NADW, LCDW and WDW (S_P~34.6-34.8, θ~0-3ºC) is evident at all latitudes as a 'knee' in the θ-S_P distribution as shown in panel A of Figure 4 in the box labelled 'Deep Waters'. Intermediate and surface waters account for the fresher and/or warmer part of the distribution, whilst the increasingly cooler and denser Weddell Sea Deep (WSDW) and Bottom Waters (WSBW) account for the remainder of the distribution. The deep and bottom waters are enlarged and labelled in panel B of Figure 4.

The salinity-maximum 'knee' successively freshens and cools polewards from the NADW to the CDW, and this pattern is present in each section used in this study and is therefore observable at all longitudes. Of particular note, however, is the reversal of this trend, where the salinity-maximum decreases from the CDW at ~55ºS (turquoise) to reach its lowest value at ~60ºS (blue), yet there are higher values further south towards 70ºS (pink). While the higher salinities around 70ºS are related to the southern limb of the Weddell Gyre which entrains LCDW in the eastern Weddell Gyre, the lowest values at ~60°S point to the Weddell Gyre centre as the final location to which the NADW can be traced by its salinity signature after circulation around Antarctica.

In order to examine the changes of the salinity-maximum along its circumpolar path it is useful to focus on the salinity-maximum data only, as shown in Figure 5. Overall there is a pattern of warm, saline NADW with a potential density of ~27.85 kg m^{-3} in the Sub-Tropical Zone of the South Atlantic (red) gradually freshening and cooling as the salinity signature moves southward and is entrained into the ACC (black). The cooling and freshening continues but the potential density remains relatively constant at ~27.80 kg m^{-3} until entrainment into the Weddell Gyre, where a more pronounced cooling results in an increase in potential density to 27.85 kg m^{-3}.

However, though it has been necessary to plot Figure 5 with contours of potential density referenced to the surface, this metric is inappropriate for the deep ocean. Whilst a deeper reference level such as 2000m would be more useful, it still fails to properly quantify the changes in density, as will be demonstrated later when examining the variability in the depth of the salinity maximum. The issue is further complicated when examining the entrainment of LCDW into the Weddell Gyre. Panel A of Figure 6 shows practical salinity plotted against potential density demonstrating the same distribution as in Figure 3. Note how the distribution changes with latitude (top) reflecting Figure 4, how the distribution changes with longitude (bottom), with the Greenwich Meridian (green) and western South Atlantic (turquoise) including the most saline NADW as well as the freshest WDW. The intermediate S_P values are present in the Indian and Pacific sectors of the Southern Ocean (blue and red). The curve of the salinity-maximum data can be seen to be centred on the value of 27.80 kg m^{-3}, with higher densities associated with NADW and WDW, and lower densities associated with the LCDW. The equivalent Neutral Density distribution shows a greater range of densities with a mean of approximately the same as for the Neutral Density surface shown in Figure 1 of γ_n = 28.05 kg m^{-3} associated with the highest salinities in the NADW and LCDW (Figure 6, panel B). The prominent spread of Neutral Density at lower salinities is associated with the WDW and this demonstrates the cross-isopycnal movement of the salinity-maximum when moving from the ACC, across the Southern Boundary/Weddell Front into the Weddell Gyre. The different perspectives offered by potential density and Neutral Density with respect to the Southern Boundary of the ACC is worthy of note for future studies.

The mechanism for this change between regions of the Southern Ocean is described in the ***appendix*** and can be summarised as being the result of cross-frontal mixing moving the salinity-maximum signature from the ACC regime to the Weddell Gyre regime, whereby there is a change in the overlying and underlying water masses and a vertical move upwards in the water column. This study is conducted under the assumption that tracking the salinity maximum along the temperature-salinity maximum curve in Figure 5 is legitimate as the changes in density are the result of real modification of the water mass as it moves from regime to regime.

A further examination of the spatial distribution and nature of the deep salinity maximum is supported by Figure 7 which shows the variation of salinity with latitude, grouped by cruises on similar longitudes. A number of key observations can be made using this figure, however care should be taken when comparing the subplots in Figure 7 as they have different axes to allow focus on different features. Firstly, when compared to other areas of the Southern Ocean, there is a relatively large variability in the salinity maximum in the Atlantic sector of the Southern Ocean north of the Weddell Gyre. This could be explained by the effect of transient eddies moving across a strong meridional gradient in the salinity maximum. In other sectors of the Southern Ocean there is no such strong meridional gradient and so the effect of eddies is not as apparent. In the Weddell Gyre, whilst it is generally considered more quiescent than the ACC, across the Greenwich Meridian eddy activity associated with Maud Rise accounts for observed variability. Secondly, the salinity maximum of the Indian sector (subplot A and dark blue - subplot B) intersects with the Atlantic sector sections at $S_P > 34.75$, latitude ~51ºS and the profile becomes convex across a reduced range in S_P. As the LCDW is drawn eastwards through the Pacific sector (light blue - subplot B) and Drake Passage (red - subplot C) the salinity maxima continues to decrease and the curve of the profile flattens. In subplot D (black and light and dark teal) the southern ACC is visible north of the Weddell Front/Southern Boundary at ~55ºS, along with the trough in S_P associated with the northern Weddell Gyre (~60ºS) and the peak of the southern Weddell Gyre (~65ºS).

It is also of interest that through the Indian and Pacific sectors the latitudinal peak in the salinity maximum gradually shifts southwards, from being at the extreme north of the sections (~50ºS) in the Indian sector to being at the extreme south of the sections (~70ºS) in the eastern Pacific. Whilst the transient eddy field may have a role in this apparent southward shift, another possible cause is vertical mixing between the more saline CDW and less saline AAIW north of the Polar Front. South of the polar front AAIW has not yet subducted and is therefore not a factor in deep ocean mixing at higher latitudes. The result of such mixing would be to enhance dilution of the LCDW in the north of the ACC compared to the south of the ACC, giving the appearance of a southward movement when instead this may simply be a latitudinal variation in vertical mixing. However, this hypothesis requires further investigation which is beyond the scope of this study.

The salinity-maximum is therefore used as a proxy for the overall impact of mixing upon the deep salinity-maximum core of the NADW, LCDW and WDW. It can be used to examine spatial and temporal variability, entrainment from one regime to another, and to estimate mixing rates along the circumpolar pathway.

3.5 - Results - Along-Path and Temporal Change

The change in the salinity-maximum along the circumpolar pathway can be seen in Figure 8a. Starting from the highest NADW salinities in the Sub-Antarctic Zone (SAZ, sections 1 & 2) of the Atlantic Sector, NADW is then entrained into the Polar Front Zone (PFZ, 3/4) producing the highest salinity maximum values along the ACC. The salinity-maximum decreases throughout the ACC in the Indian and Pacific sectors of the Southern Ocean and back through Drake Passage and into the Antarctic Zone (A23-AZ) of the Atlantic sector (sections 5-16). There is then a noticeable increase in salinity in the transition from the A23-AZ sections to the SR02-AZ sections (section 17) with the only potential source of this increase being from cross-frontal mixing with LCDW from further north across the PFZ. As the only source of higher salinity water masses in the deep - but not bottom layers – LCDW is then entrained into the WDW in the eastern Weddell Gyre, with the decrease continuing through the eastern and southern Weddell Gyre (sections 18-21). The salinity signature then increases in the northern Weddell Gyre (sections 22-24) which must be due to cross-frontal mixing with the AZ of the ACC and/or mixing with higher salinity WDW across the central axis of the Weddell Gyre.

The change in the depth of the salinity maximum is more variable than the actual salinity values, as shown in Figure 8b. The NADW values place the salinity maximum at ~2750 m depth in the Sub-Antarctic Zone, rising to ~2500 m in the Polar Front Zone of the Atlantic sector and stabilising at a depth of ~1500m across the Indian sector. The depth then fluctuates between 1500 m and 2100 m across the Pacific sector apparently due to the combined impact of the shift in the vertical distribution of water masses and topographic effects (see Figure 2 for major topographic features). In detail, the ACC fronts remain on or south of the Australian-Antarctic Ridge through the Indian sector resulting in the consistent vertical distribution of the underlying AABW and overlying AAIW, corresponding to a steady salinity-maximum depth (see section group 5-8). However, to the east of the Macquarie Ridge the fronts move to the north of the Pacific Antarctic Ridge (~3000m ridge depth) into the Southwest Pacific Basin where lower volumes of AABW are present due to topographic barriers in the northwest Ross Sea and an absence of topographic barriers to the northeast in the Bellingshausen Abyssal Plain which allows AABW to flow northwards at greater depth, resulting in the downward displacement of the salinity-maximum in the water column (sections 9 & 10). The salinity-maximum depth shallows as the ACC crosses the Pacific-Antarctic Ridge due to topographic uplift (section 11), and returns to a deeper level across the Amundsen, Bellingshausen and Mornington Abyssal Plains (sections 12-14): here it is due to the lack of topographic constraint on AABW flowing northeast out of the Ross Sea resulting in a deeper and more saline bottom water signature. The salinity-maximum shallows towards 1000 m as it moves through Drake Passage and into the Antarctic Zone of the Atlantic sector (sections 15-17). The signature finally shallows to ~500 m within the WDW of the Weddell Gyre representing the end of the shoaling of isopycnals associated with the LCDW (sections18-24).

The variability in the per-cruise mean salinity-maximum between repeat occupations of a section is often only as large as the variability of the salinity-maximum (defined as standard error of the mean) between the stations of a single cruise. This is demonstrated in Figure 9 where the section mean of the salinity-maximum is plotted with bars of standard-error to demonstrate inter- and intra-section variability.

Considering the scarcity of data in time, the less than 20-year time span for even the best sampled sections, and multi-decadal timescales of circumpolar circulation; there appears to be no significant multi-annual trend in the section mean salinity maximum of the LCDW although small increases and decreases are observed. In detail these are (numbers in brackets refer to sub-section number as per Table 1):

- The SR02-SAZ (1) salinities are surprisingly stable considering that the data sampling was regionally irregular, whilst there is actually greater variability within the SR02-PFZ (2) occupations which were more consistently surveyed. This suggests a relatively homogenous and quiescent SAZ and more variable and dynamic PFZ.
- The occupations of sections I06S (5) through to SR03 (8) show low variability between occupations of each section, and are collectively a consistently close grouping.
- The Pacific sector and Drake Passage sections (11-16) have a greater degree of variability compared to the previous group of sections, but still largely within the range of the associated error.
- The SR02-AZ (17) sections show the greatest variability, with values as high as the lowest P16S occupations and as low as the mid-range of the SR01 occupations. This suggests a variable cross-frontal influence from the PFZ, possibly the result of short-term impacts from eddy-activity. As the partition of section occupations is done on the basis of oceanographic features and not geographical position, this cannot be due to meandering of the Polar Front.

- The smaller error bars and lower inter-section variability within the northern Weddell Gyre (23), compared to the more pronounced variability of the southern Weddell Gyre (20), suggests variability in the salinity-maximum signature may be attenuated by local mixing processes in the western Weddell Gyre. The greater variability in the southern Weddell Gyre may be linked to known variability in volume transport into the region, as demonstrated by Cisewski et al. (2011), associated with jets created by the topography of Maud Rise.
- The most profound statement which can truly be made about those sections with only two occupations (1, 3, 6, 7, 11, 13 and 16) is that the repeats are not unexpectedly different, as a meanginful trend cannot be inferred from two data points.

There are three main conclusions to be drawn from these results. Firstly, there is no observable temporal trend in the value of the salinity-maximum for the time period considered. Secondly, there are clear regimes of spatial change in the value of the salinity-maximum to which a simple linear fit can be applied to determine the $\frac{\partial s}{\partial i}$ term in equation [7]. The following letters correspond to the linear fits shown in figure 8a:

A. the Sub-Antarctic Zone/Polar Front in the Atlantic sector;
B. the Indian sector/Pacific sector/Drake Passage;
C. the Antarctic Zone of the Atlantic sector, and the eastern and southern Weddell Gyre;
D. the western and northern Weddell Gyre;

Thirdly, that the depth of the salinity maximum may vary during the circumpolar transit but it maintains a stable range of density, which is only modified by significant shifts from one regime to another.

4 - Water Mass Analysis

4.1 – Water Mass Analysis Method

In an effort to quantify the relative downstream changes in the salinity maximum in terms of water mass modification, a water mass analysis has been performed for the mean of the mean salinity maxima. This is based on an inverse calculation of the θ-S_p properties of both the mean of the mean salinity maxima for each section and the mixing end members of NADW, AASW and AABW.

The mixing end members have been set according the appropriate maxima/minima available from the hydrographic datasets used in this study as follows: the highest observed salinity maximum for the NADW in the Atlantic sector (S_p = 34.884, θ = 2.762ºC); the lowest surface salinity for the AASW in the Weddell Gyre (S_p = 33.90, θ = 0ºC), and the lowest observed salinity in AABW (S_p = 34.65, θ = -0.7ºC). The output from this set of calculations is an estimate of the relative percentage contribution of each mixing end-member. However, it should be noted that as AASW and AABW have regional variations in their properties, that this is an indicative contribution during the entire circumpolar transit of LCDW reflecting the erosion of the salinity maximum and it is not an explicit contribution of AASW or AABW along any specific section.

4.2 – Water Mass Analysis Results

The results from the water mass analysis are contained in Table 2 which lists the percentage indicative contribution in θ-S_p space for each mixing end member and the percentage change from the previous up-stream section. The entrainment of NADW into the ACC between sections 1 and 5 shows an overall 32.7% decrease in NADW, a 7.6% increase in AASW and 23.9% increase in AABW, whilst the NADW contribution in SAZ of the eastern South Atlantic (section 3) is noticeably lower than in the eastern South Atlantic (section 1). These are the only sections where the AASW contribution shows a significant increase, consistent with the down welling on AASW to form AAIW at the Polar Front.

For sections 6-15 there are either small increases or small but overall significant decreases in NADW contribution, the latter consistent with the gradual erosion of the salinity maximum through the Indian and Pacific sectors. This is followed by a small increase or 2.9% in NADW contribution for sections 16 and 17 upon return to the Atlantic sector suggestive of entrainment southward across the Polar Front. When combined with the additional comparison of section 17 with section 5 where there is a 7.8% increase eastwards, this result is significant as it demonstrates the meridional barrier to transport posed by the ACC fronts acting to minimise direct meridional input from the South Atlantic to the Weddell Gyre.

There is then a large decrease (-15.3%) in NADW contribution and a large increase (17%) in AABW contribution marking the shift into the Weddell Gyre (section 18). This is followed by a minor increase suggesting that section 19 is entirely dominated by water masses circulating from the eastern Weddell Gyre. Sections 20-22 then show a renewed decrease in NADW and increase in AABW contributions consistent with further erosion of the salinity maximum throughout the southern and western and north-western Weddell Gyre, which is consistent with a net transport northward from the South Scotia Arc.

The final water mass modifications are in the northern Weddell Gyre where increasing NADW contributions indicate that entrainment occurs into the Weddell Gyre from the ACC across the Weddell Front/Southern Boundary east of the South Scotia Ridge, followed by a further 6.2% increase of NADW contribution during recirculation to section 18 and 19. This suggests that the entrainment of LCDW into the Weddell Gyre mostly occurs east of the Greenwich Meridian (5.1% + 6.2%) as opposed to the west (3.7%) by a ratio of approximately 3:1.

5 - Estimate of Mixing Coefficients

5.1 - Methods - The equation

In order to make an estimate of the rate of mixing along the path of the LCDW a diffusive-advective mixing scheme is assumed to sufficiently approximate the large-scale effects of mixing across a range of smaller scales:

$$[3]\,\frac{\partial \acute{S}}{\partial t} + u\frac{\partial \acute{S}}{\partial x} + v\frac{\partial \acute{S}}{\partial y} + w\frac{\partial \acute{S}}{\partial z} = \kappa_H\left(\frac{\partial^2 S}{\partial x^2} + \frac{\partial^2 S}{\partial y^2}\right) + \kappa_V\frac{\partial^2 S}{\partial z^2} + R$$

where

$$[4]R = \frac{-\partial}{\partial x}\left(\acute{u}S\right) - \frac{\partial}{\partial y}\left(\acute{u}S\right) - \frac{\partial}{\partial z}\left(\acute{u}S\right);$$

$\frac{\partial \acute{S}}{\partial t}$ is the change in salinity with time; u,v,w are respectively the mean zonal, meridional and vertical components of velocity; $\frac{\partial \acute{S}}{\partial x}, \frac{\partial \acute{S}}{\partial y}, \frac{\partial \acute{S}}{\partial z}$ are respectively the mean change in salinity in the zonal, meridional and vertical directions; κ_H is the horizontal mixing coefficient and κ_V is the vertical mixing coefficient; $\frac{\partial^2 S}{\partial x^2}, \frac{\partial^2 S}{\partial y^2}$, $\frac{\partial^2 S}{\partial x^2}$ are respectively the uniform rate of change in salinity gradient with respect to the zonal, meridional and vertical directions; and R represents the eddy fluxes of tracers terms as shown in [4]. Despite the turbulent nature of the Southern Ocean where mesoscale and turbulent mixing are significant, these contribute to the bulk mixing considered in this study and the terms of [3] therefore hold at scales of hundreds of kilometres.

5.2 - Methods - Assessment of terms

Using scale analysis we can determine which, if any of these terms can be neglected in calculating rates of oceanic mixing.

On the left hand side of the equation, firstly we can reasonably neglect the $\frac{\partial \acute{S}}{\partial t}$ term as this study did not identify any significant temporal trend in the deep salinity maximum (see part 3.5 and Figure 9). Whilst the absence of a trend is not conclusive, the variability between repeat occupations of sections is greater than the size of any trend, operating on the timescale for circumnavigation of Antarctica of the order of decades. Next we can neglect the $v\frac{\partial \acute{S}}{\partial y}$ term as the meridional transport across the ACC is dominated by transient eddies and is relatively small compared to the zonal transport (Marshall & Speer, 2012; Lauderdale, 2013), whilst the isopycnal salinity gradient is too small for sections outside the Atlantic sector of the ACC which are not the target for this calculation. Similarly, the $w\frac{\partial \acute{S}}{\partial z}$ term can also be neglected as vertical transport is an even smaller component than the meridional transport, and when considered within the context of shoaling isopycnals this term becomes insignificant as it is reduced to local fluctuations related to turbulence.

On the right hand side of the equation we can neglect the $\frac{\partial^2 S}{\partial x^2}$ term as it estimated to be ~10^{-16} m^{-2}, whereas the $\frac{\partial^2 S}{\partial y^2}$ is estimated at ~10^{-14} m^{-2} and therefore dominates the overall term relating to κ_H; both values have been calculated by fitting quadratic curves to the data in the ACC along path and across path directions respectively for the Indian and Pacific sectors (sections 5 to 16 in Figure 8a). In addition, despite being able to calculate the along path term, it is difficult to distinguish an eastward moving salinity maximum from the term for zonal mixing. Finally, there is insufficient information to accurately include the Reynold's Stress terms and so the effect of the terms must be implicitly included in the remaining terms. This leaves us with:

$$[5] u\frac{\partial \acute{S}}{\partial x} = \kappa_H \frac{\partial^2 S}{\partial y^2} + \kappa_V \frac{\partial^2 S}{\partial z^2}$$

However, owing to the nature of the ACC, where the isopycnal surfaces are strongly sloping, the horizontal (κ_H) mixing term is more accurately expressed as isopycnal (κ_I) mixing:

$$[6] u\frac{\partial \acute{S}}{\partial x} = \kappa_I \frac{\partial^2 S}{\partial y^2} + \kappa_V \frac{\partial^2 S}{\partial z^2}$$

Furthermore, as the path of the ACC meanders across the Southern Ocean it is inappropriate to consider the downstream flow to be strictly zonal or the rate of change in salinity across the ACC to be strictly meridional and the equation therefore becomes:

$$[7] u\frac{\partial \acute{S}}{\partial i} = \kappa_I \frac{\partial^2 S}{\partial j^2} + \kappa_V \frac{\partial^2 S}{\partial z^2}$$

Where u, the downstream velocity is obtained from the ECCO model; $\frac{\partial \acute{S}}{\partial i}$ is the downstream change in salinity obtained from an appropriate linear fit of circumpolar changes in salinity; $\frac{\partial^2 S}{\partial j^2}$ is the rate of change in salinity gradient in the across-stream direction. By collecting information on each of these terms for every appropriate section in the circumpolar transit of the LCDW an estimate of bulk mixing can be obtained for the deep ocean using a least squares linear regression. A statistical estimate of error associated with these calculated mixing terms is provided by the estimated standard error of the isopycnal and vertical mixing coefficients which is calculated as the square root of the estimated diagonal covariance matrix.

5.3 - Methods - Velocity estimates

In order to provide a representative value for u, it was essential to obtain a realistic estimate for the downstream velocity. At a basic level, if we assume an upper limit of 150 Sv transport for the ACC through Drake Passage, with a mean depth of 4000 m and an approximate width of 5° of latitude, we arrive at a mean value for u of 7.1 cm s^{-1} for the entire water column. This represents an absolute upper bound for velocities at LCDW depth which is in the lower half of the water column.

Döös (1995) estimates a mean residence time for water particles moving between the different ocean basins via the indirect ventilated route in the Southern Ocean to be 243 years. When scaled by the estimated 6 circumnavigations, it suggests a typical circumnavigation time of 40.5 years. Using an ACC circumpolar track length of order 27 000 km derived from Orsi's (1995) Polar Front; this would provide a mean current speed of 2.1 cm s^{-1}. This is an estimate for water masses at a range of mid water column depths and provides a reasonable value well within the upper limit described previously.

Another useful point of reference is the estimate of the mean tangential velocity to the path of the ACC estimated by Olbers et al. (2004). The mean estimate of Southern Ocean velocity suggests velocities ranging from 8 cm s^{-1} at depths of ~1000m, decreasing to 2 cm s^{-1} at depths of ~3000m: this is consistent with both of the above estimates.

To obtain a robust set of estimates for eastward velocities, the ECCO live access server was used to obtain velocity data for each section spanning the full range of the model solutions, from 1992 to 2008. The average (where repeat occupations occur) north and south limits defined by the section partitioning was used for the meridional limits of the ECCO data at a constant depth relevant to the average depth of the salinity-maximum for each section. A simple time-latitude average was calculated to obtain a mean velocity. This is a preferable method to calculating individual section transport velocities, say based on hydrography, as such a method would provide only snapshot estimates of velocities when the circumpolar distribution of tracers is determined by the long-term flow. Within the ACC the minimum velocity determined by this method was 1.34 cm s^{-1} in the Polar Front Zone of the A23 sections, and the maximum was 4.82 cm s^{-1} across the SR01 Drake Passage sections. As expected, overall lower velocities were determined for the Weddell Gyre, with a minimum of 0.87 cm s^{-1} in the far eastern Weddell Gyre and a maximum of 1.83 cm s^{-1} in the northern limb of the Weddell Gyre across the SR02 sections. These values are consistent with the earlier outline calculations.

5.4 - Methods - Second differentials

The terms $\frac{\partial^2 S}{\partial j^2}$ and $\frac{\partial^2 S}{\partial z^2}$ in equation [5] were estimated by calculating the second differential of a quadratic fit to the salinity data. The $\frac{\partial^2 S}{\partial j^2}$ term is obtained from a single fit to the profile of the salinity-maximum along the section. The $\frac{\partial^2 S}{\partial z^2}$ term is the mean for each section occupation of the second differential of the quadratic fit to each station salinity profile, for appropriate ranges of salinity. Within the ACC the vertical quadratic fit was obtained for $S_P > 34.68$, and for the Weddell Gyre $S_P > 34.67$. This discrimination was necessary due to the lower salinity values in the upper water column of the Weddell Gyre.

5.5 – Results - Mixing Coefficients

With reference to Equation [7], whilst all stations provided a consistently negative $\frac{\partial^2 S}{\partial z^2}$ term, the $\frac{\partial^2 S}{\partial j^2}$ term was not consistently negative across all sections. Due to the lack of distinct curvature in the cross-stream gradient of the salinity-maxima across the Polar Front and Antarctic Zones of the Atlantic sector, the computed values for $\frac{\partial^2 S}{\partial j^2}$ term were near zero, being orders of magnitude smaller than for sections in the Indian and Pacific sectors of the Southern Ocean, and varying between being positive or negative. I06S was similarly affected by the continuation of the deep salinity-maximum beneath the Agulhas Retroflection.

Additionally, I08S was affected by the presence of the Kerguelen Plateau which results in a bimodal peak in the salinity-maximum to the north and south of the plateau, with an intervening low salinity-maximum associated with the deep Australian-Antarctic Gyre (McCartney and Donohue 2007). The shallow bathymetry forces LCDW to be transported around the north and south of the plateau, as reflected in the diversion of the ACC fronts in Figure 3. The effect of this deep gyre can also be seen in the profile of one of the two occupations of I09S (Figure 7, Subplot B – seen as a dark blue low salinity spike), suggesting it has a variable zonal impact.

Finally, in the northern Weddell Gyre the term varies between positive or negative values due to the influence of the mixing with the Antarctic Zone to the north and with the southern Weddell Gyre. This also makes the downstream salinity gradient, $\frac{\partial S}{\partial i}$, term positive.

The impact of the above terms assessed for the above sections is that it renders them unsuitable for use with linear regression as the mixing equation assumes a body diffusing as it advects and does not account for additional sources of salinity. While it is therefore not possible to calculate mixing coefficients for the above mentioned sections, the SR03 and Pacific sector sections as well as the sections covering the eastern and southern Weddell Gyre are suitable for that purpose, as shown in Table 3. Within the ACC – from the SR03 sections to the A21 section – a vertical mixing coefficient is obtained of $\kappa_V = 2.86 \times 10^{-4}$ m^2 s^{-1} and an isopycnal mixing coefficient of $\kappa_I = 8.97 \times 10^2$ m^2 s^{-1}. Each has estimated standard error of the coefficients of the same order of magnitude, but numerically smaller as shown in Table 3.

In the eastern and southern Weddell Gyre the vertical mixing coefficient is an order of magnitude smaller, at $\kappa_V = 2.39 \times 10^{-5}$ m^2 s^{-1}: likely due to the general absence of significant topographic features when compared with mid-ocean ridges that lay below the ACC. The isopycnal coefficient is the same order of magnitude as for the ACC, at $\kappa_I = 2.47 \times 10^2$ m^2 s^{-1}. Whilst the κ_I has an associated error which is an order of magnitude smaller, the κ_V is not only the same order of magnitude but also numerically larger. This appears to be due to the presence of the Maud Rise seamount on the Greenwich Meridian causing increased vertical mixing compared to the rest of the Weddell Gyre, and the contrast between the rates of vertical mixing leads to a larger error.

The combined calculation places the vertical mixing coefficient at $\kappa_V = 2.86 \times 10^{-5}$ m^2 s^{-1} and associated error similar to that for the Weddell Gyre and for the same reasons. The isopycnal mixing coefficient remains at the same order of magnitude, at $\kappa_I = 2.62 \times 10^2$ m^2 s^{-1}, with the associated error an order of magnitude smaller. As the combined calculation produces coefficients which are similar to the eastern and southern Weddell Gyre coefficients, and the SR03 and Pacific sections have a much larger associated error, this suggests that there is greater variability in the vertical mixing rates in the Pacific sector than in the Weddell Gyre, with some regions of the Pacific being more quiescent than others. This is consistent with known variations in underlying bathymetry across the Pacific sector of the Southern Ocean.

Collectively, these values suggest it is best to consider the two regimes independently: in general the Weddell-Enderby Basin is bathymetrically smooth, with the exception of major features such as Maud Rise, whereas the SR03 and Pacific sector sections cross rough and complex topography, particularly to the south of Australia and New Zealand and across the Pacific Antarctic Ridge.

6 - Discussion

6.1 - Variability and Stability in the Southern Ocean

6.1.1 - Circumpolar trends

The quantitative observations made in this study about the circumpolar freshening trend of the salinity-maximum downstream from the NADW source is consistent with the brief circumpolar part of the study by Williams et al. (2006) and reinforces the earlier observations of Callahan (1972) regarding the distribution of deep water masses. Within Drake Passage, Williams et al. (2006) identify no clear trend in the core thermohaline properties of the LCDW across the entire study period between 1926 and 2004, whilst our study seems to confirm their initial assessment that there is no apparent temporal trend within the LCDW domain across the rest of the Southern Ocean either. This does not preclude a long-term trend from existing in the Southern Ocean wide deep salinity-maximum; however there is an insufficiently large hydrographic dataset at this time to judge circumpolar inter-decadal changes.

Observations of warming in the Southern Ocean suggest thermohaline changes are or were taking place. A prominent example is the 0.17 K warming between 1950 and 1980 at depths of 700-1100 m as detected by Gille (2002) and thought to be linked to the annually ventilated mode waters forced by atmospheric warming. As LCDW is predominantly deeper than this, it is entirely feasible that this temperature increase does not apply to the deeper ocean, as supported by the results of Williams et al. (2006).

The ACC in general is known to exhibit variability in flow regimes, transport and frontal positions. According to Turner and Overland (2009), certain parts of the Southern Ocean have changed rapidly in the last century, but there is a complex pattern of change, with multiple mechanisms and feedbacks implicated in the variability of ocean characteristics. They propose that the variability of LCDW water mass characteristics could be accounted for by: an acceleration in the ACC affecting entrainment of source water masses; the southward shift of the ACC and its fronts as a result of changes to the Southern Annular Mode (SAM); or greater eddy activity resulting from increased westerly winds. Such variability could account for the small changes between repeat occupations.

6.1.2 - Weddell Gyre variability

Decadal scale variations in the characteristics of the Weddell Gyre have been observed across the Greenwich Meridian with the mean salinity of the WDW observed to vary between 34.677 and 34.681 by Fahrbach et al. (2004), although the variation is within the magnitude of the systematic error due to calibration. In agreement with the assessment of this study, they judge that minor variations are likely to be real. Interestingly, Whitworth and Nowlin (1987) note persistent subtle signals, such as a mid-depth silicate maximum which they identify as being sourced from the Indian Ocean. This suggests that despite mixing over long distances in the circumpolar path and across dynamic regime boundaries, variations in deep water mass properties can be conserved and have an observable presence in the Weddell Gyre, albeit as a weaker signal.

Such observed variability may be due to time-varying transports across the topographically restricted southern Weddell Gyre. Cisewski et al. (2011) calculate a westward transport of 23.9 ± 19.9 Sv in austral summer and 93.6 ± 20.1 Sv in austral winter from two separate cruises. This large variability in volume transport was thought to be linked to gyre-scale forcing by changes in the wind stress curl and manifests itself primarily in variations in the jet structures associated with the Maud Rise seamount and the Antarctic continental slope. Thus changes in transport could lead to a pulsating propagation of salinity signals from east to west.

6.2 - The exchange of water masses

Whilst at first consideration the water mass analysis appears to be a rather simple technique, it nevertheless appears to offer a useful insight into deep water mass dynamics and supports the existing evidence regarding NADW and LCDW entrainment. Underlying the transport of the ACC are the strong zonal fronts, which according to Sokolov and Rintoul (2009a, 2009b) comprise numerous branches of the conventional ACC fronts associated with sea surface height gradients. However, whilst their analysis accounts for ~90% of the variability, the remaining variability speaks to the fact that these fronts are not always strong or continuous in time and space. This owes to the propagation of eddies across these fronts which drives entrainment from one regime to another. Paraphrasing Naveira Garabato et al. (2011), under these conditions the parallel jets lead to homogenisation of water masses between fronts, however in regions of greatest eddy transport and mixing, these fronts are 'leaky' and thus provide for cross-frontal exchange of water masses exceeding that which normally occurs along the path of the ACC. We can see from the water mass analysis how this results in a more homogenous LCDW in the Indian and Pacific sectors for each cruise when compared to the Atlantic sector which influenced by the input from the north of NADW.

6.2.1 - Reasons for entrainment of NADW into the PFZ

The complex topography which results in the northward excursion of the ACC fronts into the Argentine Basin appears to be a primary means by which NADW is entrained into the PFZ of the ACC. The meandering of the fronts and the associated eddy activity allow a higher cross-frontal transfer of water mass properties than along the rest of the SAF in the Atlantic sector, as can be seen in the southwest South Atlantic in Figure 1 where the SAF shifts to higher salinities east of Drake Passage, and by the significantly higher contributions to the PFZ in the Atlantic sector compared to the rest of the ACC as shown in Table 2. The importance of the Argentine basin in mixing has been previously noted (e.g. Peterson and Whitworth 1989, Arhan et al. 1999), and the topographically driven mechanisms for the movement of these fronts within the Scotia Sea are well described by Naveira Garabato et al. (2002).

Of less importance seem to be the more easterly sections of the SAF and – surprisingly – the Agulhas Retroflection where despite carrying a deep salinity-maximum beneath it appears to make a low contribution based on significant decrease in NADW contribution from the water mass analysis method to I06S sections. This is likely to be due to this feature contributing directly to the deep waters of Indian Ocean rather than being carried east by the ACC. We therefore conclude that the southwest Atlantic is the most important region for the entrainment of NADW. However, these same water mass estimates suggest that this region of the Southern Ocean may play a greater role in transferring the more saline salinity-maximum signal across the PF, but not directly into the Weddell Gyre.

6.2.2 - Reasons for entrainment into and insulation of the Weddell Gyre

A number of authors have identified the eastern Weddell Gyre as a region dominated by eddy activity which is thought to contribute significantly to the entrainment of CDW into the Gyre (e.g. Deacon 1979, Orsi et al. 1993, Orsi et al. 1995, Gouretski and Danilov 1993). Gouretski and Danilov (1994) describe the impact of warm core eddies from the ACC moving south into the eastern Weddell Gyre and observed that they must lead to the transport of heat and salt as the eddies decay. Whilst the ACC is in an eddy-saturated state, there are regions of greater and lesser eddy activity.

Fahrbach et al. (1994) assert that the injection of LCDW can occur through the Weddell Front (the local Southern Boundary of the ACC generated by the influence of the Antarctic Peninsula) and thus cross frontal entrainment of LCDW can potentially occur west of the Greenwich Meridian. However, as the Weddell Front is variable in intensity, injection of water masses into the northern Weddell Gyre must also be subject to variability. This factor is considered less important than the eastern Weddell Gyre region, and they assert that processes local to the Gyre, either open-ocean or coastal, are likely to play a major controlling factor on the salinity signal of the WDW. This is confirmed by the water mass estimates which suggest the eastern Weddell Gyre acts an intermediate step between the ACC and western Weddell Gyre, being an even mixture of LCDW and WDW, and which is then mixed further with the WDW through the southern limb of the Weddell Gyre.

Naveira Garabato et al. (2004b) identify that turbulent mixing is enhanced over topography and this plays a crucial role in closing the overturning circulation. A particular section of interest in this study is the 20E-NWG section in the north-eastern Weddell Gyre. The dynamic height contour we use to denote the Southern Boundary of the ACC is present only in the extreme north of the section at ~53.5ºS. The Southwest Indian Ridge underlies the front at this latitude and deepens further east, through which the ACC deflects southwards. Rough topography and a meandering ACC provide ideal conditions for turbulent mixing to act to modify the LCDW and entrain it into the eastern Weddell Gyre, and the water mass estimates in this study reinforce the concept of the eastern Weddell Gyre as a key gateway for LCDW entrainment. This view is consistent with salinity distribution determined by the objective mapping of Argo float measurements in the upper-ocean of the Weddell Gyre by Reeve et al. (2016).

6.2.3 - Water Mass Pathways

The frontal meridional barrier presented by the ACC outweighs the poleward transport of properties by eddies ensuring the downstream propagation of the deep salinity-maximum signature in the ACC dominates the deep pathway of the MOC.

This view of the Southern Ocean circulation is reflected by the particle exchange experiments of Döös (1995) which contrasts various pathways of inter-basin exchange. Our study deals with the indirect ventilated route of particles moving through the Southern Ocean, and subsequently upwelling south of the ACC. This route has a mean of six repeat circulations of Antarctica before exposure to the surface ocean, and this number is consistent with the water mass estimates for I06S - 6% larger than SR01 and 21% smaller than SR02-PFZ - which suggest a 4:1 dominance of SR01 recirculation across the Atlantic sector of the ACC. This route is in contrast to the direct, unventilated route whereby water moves from basin to basin without reaching the surface, such as the movement of CDW directly into the Pacific and Indian Oceans.

The water mass estimates combined with these considerations suggest that the frontal system acts as a meridional barrier to the propagation of NADW properties, insulating the Weddell Gyre from fluctuations in the large-scale circulation, and thus negating a direct meridional pathway across the ACC for the MOC.

6.3 - Estimating Mixing Rates

The results of a number of investigations of the mixing rates from a variety of different regimes and oceans have been published and it is pertinent to see whether the results of our calculations are in agreement with them.

6.3.1 – Comparison of vertical and diapycnal mixing rates

The mixing rates calculated by this study are now compared and contrasted with other examples of mixing rates determined by other authors to give context for examining variability of mixing rates within different Southern Ocean regimes. Our estimates are $(2.86 \pm 1.06) \times 10^{-4}$ $m^2 s^{-1}$ for vertical mixing for the eastern Indian and Pacific sectors of the ACC and $(2.39 \pm 2.83) \times 10^{-5}$ $m^2 s^{-1}$ in the Weddell Gyre. Munk's original (1966) estimate of a bulk κ_V for the Pacific interior was 1.3×10^{-4} $m^2\ s^{-1}$ which is between the quiescent Weddell Gyre and the turbulent ACC. In the Brazil Basin Polzin et al. (1997) demonstrate the spatial variability of mixing in the abyssal ocean, with $\kappa_D = 0.1 \times 10^{-4}$ $m^2\ s^{-1}$ over smooth topography, similar to this study's Weddell Gyre estimate under similarly low energy conditions. They obtain a higher estimate of 5×10^{-4} $m^2\ s^{-1}$ within 150 m of the sea floor and over rougher topography, twice as large as our mid-depth estimate for the LCDW in the ACC. Naveira Garabato et al. (2004a) obtained a range of estimates for weakly stratified Nordic Seas; at mid depths of 1500-2500m, $\kappa_V \approx 10^{-4}$ to 10^{-3} $m^2\ s^{-1}$ was dominant. Naveira Garabato et al. (2004b) likewise obtained a range of mixing rates at the bottom of Drake Passage, with higher rates above rough topography of 10^{-4} $m^2\ s^{-1}$ at 500m to 10^{-3} to 10^{-2} $m^2\ s^{-1}$ near the sea floor. The lower estimate is consistent with our ACC estimate which tracks topography during its circumpolar path. Zika et al. (2009) obtain a diapycnal mixing rate of $\kappa_D = (1 \pm 0.5) \times 10^{-4}$ $m^2\ s^{-1}$ for the entire Southern Ocean. In the Indian Ocean Sloyan (2006) calculates an abyssal diapycnal mixing rate, κ_D = 13-15 x 10^{-4} $m^2\ s^{-1}$ for the LCDW moving northward into the Perth Basin which is higher by a factor of 3 compared to our highest estimate. Likewise, Heywood et al. (2002) provide evidence for enhanced mixing over topography in the Scotia Sea with $\kappa_D = (39 \pm 10) \times 10^{-4}$ $m^2\ s^{-1}$ therefore also an order of magnitude larger than our estimate for the ACC. Sheen et al. (2013) report values for κ_V ranging from 10^{-5} $m^2\ s^{-1}$ at mid-depth to

10^{-3} m^2 s^{-1} near the bottom in the Scotia Sea based on in situ measurements and Waterman et al. (2013) have similar results near Kerguelen. Watson (2013) examined mixing in the UCDW using an open-ocean tracer release of trifluoromethyl sulphur pentafluoride and found κ_D to vary from ~2 x 10^{-5} m^2s^{-1} in the southeast Pacific sector of the ACC, increasing to ~7 x 10^{-5} m^2s^{-1} in Drake Passage. Lower values in the topographically deep and smooth southeast Pacific are similar to our own Weddell Gyre estimates, whilst the Drake Passage estimates is significantly lower than our SR03 and Pacific sector estimate where there is rough topography south of Australia and New Zealand. From studies on vertical mixing in the upper pycnocline performed within two transient mesoscale eddies in the Atlantic sector of the ACC, Cisewski et al. (2005, 2008) obtained K_V = 7 x 10^{-4}-10^{-3} m^2 s^{-1} with high variability of K_V on horizontal and temporal scales of order 10 km and days, respectively. For one of the eddies studied by Cisewski et al. (2008), but using a different method based on mean changes occurring over weeks in the eddy core, Hibbert et al. (2009) estimate a maximum K_V = 3 x 10^{-4} m^2 s^{-1} which is well within our own ACC estimate. A more recent study by Ledwell et al. (2011) diagnosed a diapycnal diffusivity $\kappa_D = (1.3 \pm 0.2)$ x 10^{-5} m^2 s^{-1} in the eastern Pacific sector of the ACC averaged over 1 year and thousands of kilometres: a value which is characteristic of the mid-latitude ocean interior. Given the less rough topography of the region this value fits better with our estimate for the relatively quiescent Weddell Gyre, rather than our ACC estimate. Finally, Leach et al. (2011) obtained the very low diapycnic diffusivity of 3 x 10^{-6} m^2 s^{-1} in the westward flowing southern limb of the Weddell Gyre.

The consensus seems to be that in general a value for k_v of 10^{-4} m^2 s^{-1} is typical for the ocean in general with lower values of 10^{-5} m^2 s^{-1} in quieter regions and 10^{-3} m^2 s^{-1} or larger near topography or in the upper ocean, and our values are consistent with this.

6.3.2 - Horizontal and isopycnal mixing

An early estimate for horizontal mixing by Munk (1950) required κ_H = 5 x 10^3 m^2 s^{-1} in order to obtain a realistic scale for the western boundary current of a wind driven gyre, but Okubo (1971) reviewed estimates of horizontal eddy diffusivities and found that they were scale-dependent. Ledwell et al. (1998) based on a tracer-release experiment in the eastern North Atlantic estimated values of 2 m^2 s^{-1} for scales of 1–10 km increasing to 1000 m^2 s^{-1} for scales of 30–300 km. Cunningham and Haine (1995) obtained a value of 950 m^2 s^{-1} and a scale of 166 km for the core of the Labrador Sea Water in the North Atlantic. Zika et al. (2009) obtained an isopycnal mixing rate of $\kappa_I = 300 \pm 150$ m^2 s^{-1} for the entire Southern Ocean, while Hibbert et al. (2009) also estimated a K_H = 30-100 m^2 s^{-1} within a cold core eddy. Leach et al. (2011) examined mixing of the WDW entering the

Weddell Sea with the south-eastern limb of the Weddell Gyre across the Greenwich Meridian and found an isopycnal diffusivity of 70-140 $m^2 s^{-1}$. Our estimate of 897 ± 167 $m^2 s^{-1}$ for isopycnal mixing in the ACC is consistent with values for scales larger than that of individual eddies. Our smaller Weddell Gyre value of 247 ± 63 $m^2 s^{-1}$ is perhaps more consistent with Leach et al. (2011), who also had smaller values here, possibly due to weaker eddy activity.

7 - Conclusion

Motivated by the need to better understand changes in the LCDW - the water mass that represents the link between the NADW and the AABW in the Southern Ocean, and which is therefore intimately involved in closing the lower limb of the global overturning circulation - this study quantifies the spatial trend of the deep salinity-maximum that is associated with the LCDW. This is conducted within a framework of variable density regimes to the north of, within and to the south of the ACC owing to water mass modification during the process of entrainment from one regime to another. There is no observable temporal trend from the repeat occupations of sections, however there is a clear spatial pattern in the salinity signature.

This signature originates from a water mass formed in the North Atlantic, the NADW, which is transported southwards and is subsequently entrained into the ACC as LCDW. The salinity signature weakens due to freshening as it is carried through the Indian and Pacific sectors of the Southern Ocean, subject to mixing with the intermediate and bottom water masses above and below, respectively. The signature is transported through Drake Passage and the Scotia Sea, after which it remixes to some extent with NADW in the Polar Front Zone of the ACC causing a slight increase in salinity. The signature then continues to freshen after entrainment into the eastern and southern limbs of the Weddell Gyre, before undergoing a weak increase in salinity in the northern Weddell Gyre. This is due to lateral mixing with more saline waters in the ACC and the southern limb of the Weddell Gyre, to the north and south respectively. This overall decreasing trend in salinity suggests that the ACC insulates the Weddell Gyre from short-term fluctuations in the characteristics of NADW in the South Atlantic.

This assertion is supported by the water mass analysis which indicates low-levels of cross-frontal mixing, particularly evident within the western Atlantic sector. The water mass analysis estimates also suggest that there are varying degrees of entrainment from the ACC into the Weddell Gyre at all of the observed longitudes in the Atlantic sector, but that the greatest entrainment occurs within the eastern limb of the Weddell Gyre.

Estimates of vertical and isopycnal mixing coefficients are in line with other estimates for the Southern Ocean, although they are only valid for the Indian and Pacific sectors, and the eastern and southern Weddell Gyre. Two separate estimates for these two regional sets produce understandable differences: the ACC has higher mean transport velocities and flows over rougher topography than the slower moving Weddell Gyre, corresponding to higher and lower rates of vertical mixing, respectively.

The overall view that emanates from this study, summarised in Figure 10, is that the ACC acts as a long-term ‘oceanic blender’ with the blending action concentrated in the Atlantic sector. Cross-frontal mixing of NADW into the Polar Front Zone is most prominent in the Argentine Basin, with mixing across the length of the Sub-Antarctic Front elsewhere in the South Atlantic being of secondary importance. East of the Greenwich Meridian mixing across the Polar Front and the Antarctic Front appear more prominent, however there is a clear lack of a direct meridional overturning pathway in the Atlantic Sector of the Southern Ocean. Further study of the mixing of NADW/LCDW/WDW across the fronts of the ACC is warranted to further clarify the distribution of exchanges and to enhance understanding of the climatic implications for variability in the deep waters of the Southern Ocean.

Appendix

The LCDW in the ACC exists at a fairly constant neutral density layer of 28.04-28.08 kg m^{-3} throughout its circumpolar journey as earlier detailed. However, when LCDW is entrained into the Weddell Gyre as WDW the salinity maximum associated with the LCDW and WDW shallows dramatically and moves to deeper density levels. A simple 1-dimensional model is used to illustrate how the transport of the LCDW/WDW and its interaction with overlying and underlying water masses act to modify the density profile of the water column and help explain why, outside of the ACC regime, the tracking of the salinity maximum remains an acceptable technique for assessing water mass changes in the LCDW/WDW throughout its Southern Ocean journey.

Imagine that a column of water is being carried along by the ACC and as it does so it is slowly being drawn southwards towards Antarctica, whilst mixing with the overlying and underlying water masses. As a result of the poleward movement, the characteristics of these boundary water masses will change. The northward Ekman transport – out of the Weddell Gyre – results in near-surface waters occupying a shallower depth range south of the ACC. This includes the absence of AAIW which only subducts north of the Polar Front within the ACC (Sallée et al. 2010).

Dense water which forms over the Antarctic continental shelf mixes with deeper waters as it descends the continental slope to the deep ocean. This leads to the formation of topographically constrained WSDW ($-0.7^{o}C < \theta < 0^{o}C$) and WSBW ($\theta < -0.7^{o}C$) (Fahrbach et al. 1995, Gordon et al. 2001), the former of which is present at depths as shallow as 1100m compared to the salinity maximum of the LCDW in the ACC which can lie at depths of up to 2500m. The presence of WSDW and WSBW acts to force the LCDW/WDW upwards from beneath, resulting in the shoaling of isopycnals and the rise of LCDW/WDW in the water column.

The standard framework for considering the ACC includes transport being dominated by streamlines of eastward flow aligned with the position of circumpolar fronts and a strong dependence on the sloping isopycnal surfaces associated with these fronts for tracking conservative tracers. This is against the background of a northward Ekman transport near the surface and an opposing southward flux below by the mesoscale eddy field. However, whilst this approach is suitable for the ACC, the Weddell Gyre represents a different dynamical regime characterised by the recirculation of gyre water masses, water mass transformation, and interaction with the ACC along the northern and eastern boundaries of the Gyre. This appendix explores a simple example to explain the observed changes in the properties of the LCDW as it circulates around Antarctica and is entrained into the Weddell Gyre.

To provide realistic initial conditions, the hydrographic profile from station 25, cast 1 of the 2002 A12 cruise track undertaken during *FS Polarstern's* expedition ANT-XX/2 was used as the starting hydrographic profile. The station was located at 49ºS, 2.8ºE placing it south of the Sub-Antarctic Front but north of the Polar Front.

At the surface boundary, the sea surface temperature decreases by 0.005 K per time step to represent the decreasing surface temperature moving towards Antarctica, whilst the sea surface salinity is constant to represent the general stability and relative freshness of the Antarctic Surface Water. The potential temperature at the bottom boundary of 4000m decreases by 0.0018 K per time step and the salinity decreases by 0.00005 per time step, mimicking the transition into the WSBW/WSDW regime at depth.

These linear changes were derived from the total meridional temperature and salinity gradient over the A12 section as a representative trend for surface and bottom waters. As both surface and bottom waters are formed locally in the Southern Ocean, these boundary conditions provide a reasonable first order approximation to the meridional gradient in oceanographic conditions, although clearly this is an idealized approach.

In the vertical, the grid was set at 101 depth levels, spaced every 40m from 0m to 4000m. The initial A12 profile was used for the model down to a depth of 4000m (of a total cast depth of 4090m), whilst the shallowest data (at 9 dbar) was used as the surface value. Except the surface values there were no missing data.

The 1-dimensional model is based around simple equations for the modification of potential temperature and salinity:

$$[8]\theta_t = \theta_{t-1} + \frac{d\theta}{dt}\Delta t, where \frac{d\theta}{dt} = \kappa_z \frac{(\theta_{i-1} - 2\theta_i + \theta_{i+1})}{(\Delta z)^2} + w\frac{\theta_i - \theta_{i-1}}{\Delta z}$$

$$[9]S_t = S_{t-1} + \frac{dS}{dt}\Delta t, where \frac{dS}{dt} = \kappa_z \frac{(S_{i-1} - 2S_i + S_{i+1})}{(\Delta z)^2} + w\frac{S_i - S_{i-1}}{\Delta z}$$

where θ is potential temperature, S is practical salinity, t is time, i is the vertical counter, positive downwards, z is the vertical co-ordinate, positive downwards, κ_z is the diapycnal diffusivity coefficient, w is the uplift rate, Δt is the time step and Δz the vertical grid spacing.

A 120 year transport duration was derived from an estimated 40000 km track from the station location in the ACC eastward around Antarctica, subsequently returning to a more southerly position on the Greenwich Meridian, and finally entrainment into the Weddell Gyre at an assumed 1 cm s^{-1}, rounded down to the nearest whole year. The number of time steps was set at 365 and the time step size set to 120 days for a simple scaling of the duration. This is consistent with the distances and times discussed in the main body of this text, whereby LCDW is shown to recirculate in the ACC before entering the polar gyres.

The vertical thermal diffusivity coefficient, κ, was set to 5 x 10^{-5} m^2 s^{-1} which falls within the range of many studies of vertical mixing in the ocean (e.g. Munk 1966, Naveira Garabato et al. 2004b, Zika et al. 2009). In addition, to represent the rise of LCDW/WDW in the water column as a result of Ekman suction, a rate of water column uplift of 20 m yr^{-1} was applied.

Both potential density and Neutral Density were calculated based upon the new potential temperature, practical salinity and pressure at each time step.

The initial and final profiles of the 1-D model shows: an overall decrease in temperature at all depths; a marked increase in salinity in the upper water column but a slight decrease in deeper waters resulting in the upward shift of the salinity maximum; and an overall increase in the density of the profile.

The salinity and Neutral Density time-series section shown in Figure 11 illustrates the rapid upward shift of the salinity maximum as the profile moves into the modelled regime of the Weddell Gyre. Salinity stabilises at depth reflecting the shallow salinity gradient in the WSDW and WSBW whilst a fresh surface layer is retained. The potential temperature (not shown) decreases steadily at all depths, with the temperature maximum remaining at about 100m depth.

Neutral Density increases at depth resulting in a decreasingly stratified deep water column, whilst the surface boundary constraint results in a strongly stratified upper water column. The key result is that density increases at depth such that the salinity maximum initially uplifts at a similar rate to the neutral surfaces until about year 70 when the density at the salinity maximum increases whilst the depth of the salinity maximum stabilises at about 400m depth after 80 years. The intervening period represents the entrainment of the water mass into the Weddell Gyre proper.

The framework for examining the ACC described earlier is well established, however, this framework does not extend to the transition to the hydrographic regime of the Weddell Gyre (Schröder and Fahrbach 1999).

This 1-D model shows an initial decrease in the depth of LCDW from ~2500m to ~400m, paralleling the north-south distribution of temperature, salinity and density evident on sections crossing the ACC into the Weddell Gyre.

Whilst simple, this model – when viewed as a representation of the mean-state of more complex Southern Ocean dynamics over long time scales – serves to illustrate the broad-scale effect of crossing from one regime to another upon the core of the LCDW. The core of a traditional tracer can be mixed and advected over multi-year time scales to produce a result which is consistent with observations. Whilst within the core of the ACC the salinity maximum remains within a constant density layer, this is not the case as the regime shifts from a circumpolar flow to the Weddell Gyre circulation. The normal framework for examining the ACC on streamlines and isopycnal surfaces does not apply beyond the Southern Boundary of the ACC, where complicated processes of advection, mesoscale eddies and frontal meandering together modify the water column. Recognition must be given to the effects of the contrasting hydrographic regimes of the ACC and Weddell Gyre, which demonstrate a situation in which the signal of the deep salinity maximum crosses isopycnal surfaces.

Acknowledgements

This work was funded by the National Environment Research Council through a PhD Studentship at the University of Liverpool in partnership with the Alfred Wegener Institute.

Our thanks go to the scientists and crews of the various cruises whose data we have used, and to the CLIVAR and Carbon Hydrographic Data Office for hosting the publicly available data.

The state estimates were provided by the ECCO Consortium for Estimating the Circulation and Climate of the Ocean funded by the National Oceanographic Partnership Program (NOPP).

This work has been greatly improved by the comments of the initial two anonymous reviewers, and also subsequent comments from Dr. Elizabeth Jones. We also thank the final two anonymous reviewers for their contribution.

Table Captions

Table 1 – Details of cruises used from the CCHDO database. Partitioned sections denoted with the accompanying symbols *, ^, # in column 4 are only occupied by the correspondingly marked sections in column 5. All other non-marked sections are covered by all occupations.

Table 2 - Results of the water mass analysis listing: section number and name in columns 1 and 2 match those listed in Table 1 for reference; indicative percentage contributions from mixing end members of NADW, AASW and AABW in columns 3, 5 and 7 with the darkest green indicating greatest water mass contribution and white denoting lowest water mass contribution; and the change in indicative contribution since the previous section in columns 4, 6 and 8, where blue denotes a negative change, red a positive change and white no change. The change in indicative contribution for section numbers 2 and 4 are relative to the indicative contributions for section numbers 1 and 3 respectively. Heavy black lines denote shifts in regime from large decreases in NADW (sections 1-5), to overall small decreases in NADW (sections 6-15), to small increases in NADW (sections 16 and 17), back to mostly large decreases in NADW (sections 18-22), and finally large increases in NADW (sections 23 and 24).

Table 3 – Results of 3 multiple linear regression calculations based on a given number of section realisations (#) providing estimates of the vertical mixing coefficient (κ_V) and isopycnal mixing coefficient (κ_I).

Figure Captions

Figure 1 – Salinity on the 28.05 kg m^{-3} Neutral Density surface from the World Ocean Atlas 2009 with the major fronts (black lines and grey highlighted labels) and zones (brown highlighted labels) as follows: Sub-Tropical Front (STF), Sub-Antarctic Front (SAF), Polar Front (PF), Southern ACC Front (SACCF), Southern Boundary (SB), Sub-Tropical Zone (STZ), Sub-Antarctic Zone (SAZ), Polar Front Zone (PFZ), Antarctic Zone (AZ), Weddell Gyre (WG) and Ross Gyre (RG). The highest salinity values are found in the South Atlantic, decreasing eastwards through the Indian Ocean, reaching minima to the north of the ACC in the Pacific Ocean and to the south of the ACC in the high Southern Ocean. The edge of white areas indicates the intersection of the Neutral Density surfaces with the seafloor.

Figure 2 - Major bathymetric features of the Southern Ocean. The following abbreviations have been used: Basins and seas: Amundsen Abyssal Plain (AAP), Amundsen Sea (AS), Bellingshausen Abyssal Plain (BAP), Mornington Abyssal Plain (MAP), Prydz Bay (PB). Major ridge systems: Mid-Atlantic Ridge (MAR), Southwest Indian Ridge (SWIR), Kerguelen Plateau (KP), Southeast Indian Ridge (SEIR), Pacific-Antarctic Ridge (PAR), North Scotia Ridge (NSR), South Scotia Ridge (SSR), American-Antarctic Ridge (AAR), Drake Passage (DP), Falkland Escarpment (FE). Smaller bathymetric features: Maud Rise (MR), Astrid Ridge (AR), Gunneras Ridge (GR), Conrad Rise (CR), Del Cano Rise (DCR), Macquarie Ridge (MacR), Balleny Islands (BI), Balleny Islands Fracture Zone (BIFZ), Udintsev Fracture Zone (UFZ), Eltanin Fracture Zone (EFZ). North to south, the Sub-Antarctic Front, Polar Front, Southern ACC Front and Southern Boundary from Orsi et al. (1993) are displayed as yellow lines

Figure 3 – Distribution of all cruise stations used in this study (blue dots) with corresponding sections names. Fronts from Orsi et al. (1995) are shown to illustrate the extent of the ACC: Southern Boundary (green), Southern ACC Front (yellow), Polar Front (black) and Sub-Antarctic Front (red). The Polar Front is used to calculate the circumpolar path length of the ACC. The estimated path for the Weddell Gyre is shown in grey.

Figure 4 – Potential temperature-practical salinity plot coloured by latitude for the A12-1992 cruise along the Greenwich Meridian. Black boxes denote the following water masses: WSBW ($\theta < -0.7°C$); WSDW ($0°C < \theta < -0.7°C$); Deep Waters including the NADW, UCDW, LCDW and WDW ($\theta > 0°C$, $S_P > 34.6$). AABW is the deepest end-member of the circumpolar water masses. The general distributions of intermediate and surface waters are shown, including AASW.

Figure 5 – Conservative Temperature-Absolute Salinity plot for all deep salinity-maximum values from all cruises showing the relative distribution according to regimes of the Sub-Antarctic Zone and Sub-Tropical Zone (red), ACC (black) and Weddell Gyre (blue). The potential density surfaces are marked by dotted lines.

Figure 6 – The variability of all the deep salinity-maximum values from all cruises versus: A) potential density referenced to the surface and B) Neutral Density. Data points are coloured by latitude (positive northwards) in the top panel and by longitude (positive eastward) in the bottom panel.

Figure 7 - Main plot: The deep salinity maximum (Smax) associated with the NADW, LCDW and WDW for 39 cruises, with subplots for specific regions. Subplot A (green dashed box): Smax of Indian Ocean sections including SR03 repeat sections. Subplot B (blue dashed box): Smax of sections in Pacific sector of the Southern

Ocean (western Pacific: dark blue, eastern Pacific: light blue). Subplot C (red dashed box): Smax of 4 sections in Drake Passage. Subplot D (teal dashed box): Smax of sections in the Atlantic sector of the Southern Ocean focused on the Weddell Gyre (western Weddell Gyre: light teal, central Weddell Gyre: dark teal, eastern Weddell Gyre: blue).

Figure 8 – Downstream spatial change of the salinity-maximum, with distances referenced to the Greenwich Meridian. Red vertical lines and labels denote the different sectors of the Southern Ocean under consideration, with a distinction between two different zones of the northern Atlantic Sector and two different regimes in the Weddell Gyre. Numbers are in accordance with Table 1 referring to section groups as follows: 1) A23-SAZ, 2) SR02-SAZ, 3) A23-PFZ, 4) SR02-PFZ, 5) I06S, 6) I08S, 7) I09S, 8) SR03, 9) P14S, 10) P15S, 11) P16S, 12) P18, 13) P19S, 14) A21, 15) SR01, 16) A23-AZ, 17) SR02-AZ, 18) I06S-EWG, 19) 20E-SWG, 20) SR02-SWG, 21) A23-SWG, 22) A23-NWG, 23) SR02-NWG and 24) 20E-NWG.

a) Variation in the value of the salinity-maximum. The letters refer to the lines of best fit for the (A) Polar Front Zone; (B) Pacific/Indian/Atlantic western AZ Sectors; (C) Atlantic eastern AZ, Eastern & Southern Weddell Gyre; and (D) Western & Northern Weddell Gyre, with the slope of each fit shown inset.

b) Variation in the pressure/depth of the salinity-maximum.

Figure 9 – Temporal distribution of the salinity maximum for each set of repeat occupations of a section group. The numbering and naming of section groups in the key is in accordance with Table 1 and Figure 8, omitting sections with only one available occupation. Error bars are the standard error of the mean of the maximum salinity values for each section occupation. A mix of solid, dashed and dot-dash lines is used to distinguish sections along with colour. Note the change of scale at $S_P = 34.77$ to help examine detail in the ACC and Weddell Gyre.

Figure 10 – Schematic of the propagation of the deep salinity-maximum through the Southern Ocean. NADW flows southwards into the South Atlantic [1] and is entrained into the Polar Front Zone (PFZ) of the Antarctic Circumpolar Front (ACC) in the Argentine Basin [2] as Lower Circumpolar Deep Water (LCDW). LCDW is advected eastwards by the ACC, with limited cross-frontal mixing with the Antarctic Zone (AZ) in the Atlantic sector. LCDW passes through the Pacific and Indian sectors [3], during which a gradual flux of salinity carried pole ward by eddies crosses the zonal fronts. The recirculating LCDW meets the entraining NADW east of Drake Passage in the north of the ACC, whilst the LCDW is slowly entrained into the northern limb of the

Weddell Gyre to the south of the ACC [4]. The dominant entrainment of LCDW occurs in the eastern limb of the Weddell Gyre, where it is modified to Warm Deep Water (WDW) and repeatedly recirculated within the gyre until local water mass modification exports the WDW as Antarctic Intermediate Water or Antarctic Bottom Water.

Figure 11 – Time-series contour plot for the top 2500 m of the water column showing the upward migration of the LCDW salinity core (filled-colour contours) and the shoaling of Neutral Density (γ_n) surfaces towards the surface (black contour lines).

References

Arhan M, Heywood KJ, King BA (1999) The deep waters from the Southern Ocean at the entry to the Argentine Basin. Deep Sea Research Part II: Topical Studies in Oceanography 46:475-499 doi:http://dx.doi.org/10.1016/S0967-0645(98)00110-6

Bindoff NL, Rosenberg MA, Warner MJ (2000) On the circulation and water masses over the Antarctic continental slope and rise between 80 and 150°E. Deep Sea Research Part II: Topical Studies in Oceanography 47:2299-2326

Callahan JE (1972) The structure and circulation of deep water in the Antarctic. Deep Sea Research and Oceanographic Abstracts 19:563-575 doi:10.1016/0011-7471(72)90040-x

Cisewski B, Strass VH, Leach H (2011) Circulation and transport of water masses in the Lazarev Sea, Antarctica, during summer and winter 2006. Deep Sea Research Part I: Oceanographic Research Papers 58:186-199 doi:10.1016/j.dsr.2010.12.001

Cisewski B, Strass VH, Losch M, Prandke H (2008) Mixed layer analysis of a mesoscale eddy in the Antarctic Polar Front Zone. Journal of Geophysical Research-Oceans 113:19 doi:C0501710.1029/2007jc004372

Cisewski B, Strass VH, Prandke H (2005) Upper-ocean vertical mixing in the Antarctic Polar Front Zone. Deep Sea Research Part II: Topical Studies in Oceanography 52:1087-1108 doi:10.1016/j.dsr2.2005.01.010

Cunningham SA. Haine TWN (1995) Labrador Sea Water in the Eastern North Atlantic. Part II: Mixing dynamics and the advective-diffusive balance. Journal of Physical Oceanography 25:666-678 doi:10.1175/1520-0485(1995)025%3C0666:LSWITE%3E2.0.CO;2

Deacon GER (1979) The Weddell gyre. Deep Sea Research Part A Oceanographic Research Papers 26:981-995 doi:http://dx.doi.org/10.1016/0198-0149(79)90044-X

Döös K (1995) Interocean exchange of water masses. Journal of Geophysical Research: Oceans 100:13499-13514 doi:10.1029/95jc00337

Fahrbach E, Rohardt G, Scheele N, Schröder M, Strass V, Wisotzki A (1995) Formation and discharge of deep and bottom water in the northwestern Weddell Sea. J Mar Res 53:515-538 doi:10.1357/0022240953213089

Fahrbach E, Hoppema M, Rohardt G, Schröder M, Wisotzki A (2004) Decadal-scale variations of water mass properties in the deep Weddell Sea. Ocean Dynamics 54:77-91 doi:10.1007/s10236-003-0082-3

Fahrbach E, Rohardt G, Schröder M, Strass V (1994) Transport and structure of the Weddell Gyre. Annales Geophysicae 12:840-855

Gille ST (2002) Warming of the Southern Ocean since the 1950s. Science 295:1275-1277

Gladyshev S, Arhan M, Sokov A, Speich S (2008) A hydrographic section from South Africa to the southern limit of the Antarctic Circumpolar Current at the Greenwich meridian. Deep-Sea Research Part I-Oceanographic Research Papers 55:1284-1303 doi:10.1016/j.dsr.2008.05.009

Gordon AL, Visbeck M, Huber B (2001) Export of Weddell Sea Deep and Bottom Water. Journal of Geophysical Research-Oceans 106:9005-9017

Gouretski VV, Danilov AI (1993) Weddell Gyre: structure of the eastern boundary. Deep Sea Research Part I: Oceanographic Research Papers 40:561-582 doi:http://dx.doi.org/10.1016/0967-0637(93)90146-T

Gouretski VV, Danilov AI (1994) Characteristics of warm rings in the African sector of the Antarctic Circumpolar Current. Deep Sea Research Part I: Oceanographic Research Papers 41:1131-1157 doi:http://dx.doi.org/10.1016/0967-0637(94)90037-X

Heywood KJ, Naveira Garabato AC, Stevens DP (2002) High mixing rates in the abyssal Southern Ocean. Nature 415:1011-1014

Hibbert A, Leach H, Strass V, Cisewski B (2009) Mixing in cyclonic eddies in the Antarctic Circumpolar Current. J Mar Res 67:1-23

Lauderdale J, Naveira Garabato AC, Oliver KIC, Follows MJ, Williams RG (2013) Wind-driven changes in Southern Ocean residual circulation, ocean carbon reservoirs and atmospheric CO2. Clim Dyn 41: 2145. doi:10.1007/s00382-012-1650-3

Leach H, Strass V, Cisewski B (2011) Modification by lateral mixing of the Warm Deep Water entering the Weddell Sea in the Maud Rise region. Ocean Dynamics 61:51-68 doi:10.1007/s10236-010-0342-y

Ledwell JR, St. Laurent LC, Girton JB, Toole JM (2011) Diapycnal Mixing in the Antarctic Circumpolar Current. Journal of Physical Oceanography 41:241-246 doi:10.1175/2010jpo4557.1

Ledwell JR, Watson AJ, Law CS (1998) Mixing of a tracer in the pycnocline. Journal of Geophysical Research-Oceans 103:21499-21529

Lenn YD, Wiles PJ, Torres-Valdes S, Abrahamsen EP, Rippeth TP, Simpson JH, Bacon S, Laxon SW, Polyakov I, Ivanov V, Kirillov S (2009) Vertical mixing at intermediate depths in the Arctic boundary current. Geophysical Research. Letters 36:L05601 doi:10.1029/2008GL036792.

Marshall J, Speer K (2012) Closure of the meridional overturning circulation through Southern Ocean upwelling. Nature Geoscience 5, 171-180

McCartney MS, Donohue KA (2007) A deep cyclonic gyre in the Australian-Antarctic Basin. Progress In Oceanography 75:675-750

Meredith MP, Hogg AM (2006) Circumpolar response of Southern Ocean eddy activity to a change in the Southern Annular Mode. Geophysical Research Letters 33 doi:10.1029/2006gl026499

Meredith MP et al. (2011) Sustained monitoring of the Southern Ocean at Drake Passage: Past achievements and future priorities. Rev. Geophys., 49, RG4005, doi:10.1029/2010RG000348

Moore JK, Abbott MR, Richman JG (1999) Location and dynamics of the Antarctic Polar Front from satellite sea surface temperature data. Journal of Geophysical Research: Oceans 104:3059-3073 doi:10.1029/1998jc900032

Munk WH (1950) On the wind-driven ocean circulation. Journal of Meteorology 7:80-93 doi:10.1175/1520-0469(1950)007<0080:otwdoc>2.0.co;2

Munk WH (1966) Abyssal recipes. Deep Sea Research and Oceanographic Abstracts 13:707-730 doi:10.1016/0011-7471(66)90602-4

Naveira Garabato AC, Ferrari R, Polzin KL (2011) Eddy stirring in the Southern Ocean. Journal of Geophysical Research: Oceans 116:C09019 doi:10.1029/2010jc006818

Naveira Garabato AC, Heywood KJ, Stevens DP (2002) Modification and pathways of Southern Ocean Deep Waters in the Scotia Sea. Deep Sea Research Part I: Oceanographic Research Papers 49:681-705 doi:10.1016/s0967-0637(01)00071-1

Naveira Garabato AC, Oliver KIC, Watson AJ, Messias M-J (2004a) Turbulent diapycnal mixing in the Nordic seas. Journal of Geophysical Research: Oceans 109:C12010 doi:10.1029/2004jc002411

Naveira Garabato AC, Polzin KL, King BA, Heywood KJ, Visbeck M (2004b) Widespread Intense Turbulent Mixing in the Southern Ocean. Science 303:210-213 doi:10.1126/science.1090929

Okubo A (1971) Oceanic diffusion diagrams. Deep Sea Research and Oceanographic Abstracts 18:789-802 doi:http://dx.doi.org/10.1016/0011-7471(71)90046-5

Olbers D, Borowski D, Völker C, Wölff J-O (2004) The dynamical balance, transport and circulation of the Antarctic Circumpolar Current. Antarctic Science 16:439-470 doi:doi:10.1017/S0954102004002251

Orsi AH, Nowlin Jr WD, Whitworth III T (1993) On the circulation and stratification of the Weddell Gyre. Deep Sea Research Part I: Oceanographic Research Papers 40:169-203 doi:http://dx.doi.org/10.1016/0967-0637(93)90060-G

Orsi AH, Whitworth III T, Nowlin Jr WD (1995) On the meridional extent and fronts of the Antarctic Circumpolar Current. Deep Sea Research Part I: Oceanographic Research Papers 42:641-673 doi:http://dx.doi.org/10.1016/0967-0637(95)00021-W

Patterson SL, Whitworth II T (1990) Physical oceanography, in *Antarctic Sector of the Pacific*, edited by G.P. Glasby pp. 55-93, Elsevier, New York

Peterson RG, Whitworth III T (1989) The subantarctic and polar fronts in relation to deep water masses through the southwestern Atlantic. Journal of Geophysical Research: Oceans 94:10817-10838 doi:10.1029/JC094iC08p10817

Polzin KL, Toole JM, Ledwell JR, Schmitt RW (1997) Spatial variability of turbulent mixing in the abyssal ocean. Science 276:93-96 doi:10.1126/science.276.5309.93

Purkey SG, Johnson GC (2010) Warming of global abyssal and deep Southern Ocean waters between the 1990s and 2000s: Contributions to global heat and sea level rise budgets. Journal of Climate 2, 6336–6351

Reeve K, Boebel O, Kanzow T, Strass V, Rohardt G, Fahrbach E (2016) A gridded data set of upper-ocean hydrographic properties in the Weddell Gyre obtained by objective mapping of Argo float measurements. Earth System Science Data, 8 (1), pp. 15-40. doi:10.5194/essd-8-15-2016

Rhein M, Stramma L, Krahmann G (1998) The spreading of Antarctic bottom water in the tropical Atlantic. Deep Sea Research Part I: Oceanographic Research Papers 45:507-527 doi:http://dx.doi.org/10.1016/S0967-0637(97)00030-7

Sallée JB, Speer K, Rintoul S, Wijffels S (2010) Southern Ocean Thermocline Ventilation. Journal of Physical Oceanography 40:509-529 doi:10.1175/2009jpo4291.1

Schröder M, Fahrbach E (1999) On the structure and the transport of the eastern Weddell Gyre. Deep Sea Research Part II: Topical Studies in Oceanography 46:501-527

Sheen KL, Brearley JA, Naveira Garabato AC, Smeed DA, Waterman S, Ledwell JR, Meredith MP, St. Laurent L, Thurnherr AM, Toole JM, Watson AJ (2013) Rates and mechanisms of turbulent dissipation and mixing in the Southern Ocean: Results from the Diapycnal and Isopycnal Mixing Experiment in the Southern Ocean (DIMES). Journal of Geophysical Research: Oceans: 118:2774–2792 doi:10.1002/jgrc.20217.

Sloyan BM (2006) Antarctic bottom and lower circumpolar deep water circulation in the eastern Indian Ocean. Journal of Geophysical Research: Oceans 111:C02006 doi:10.1029/2005jc003011

Sokolov S, Rintoul SR (2009a) Circumpolar structure and distribution of the Antarctic Circumpolar Current fronts: 1. Mean circumpolar paths. Journal of Geophysical Research-Oceans 114 doi:10.1029/2008jc005108

Sokolov S, Rintoul SR (2009b) Circumpolar structure and distribution of the Antarctic Circumpolar Current fronts: 2. Variability and relationship to sea surface height. Journal of Geophysical Research-Oceans 114 doi:10.1029/2008jc005248

Speer KG, Zenk W (1993) The Flow of Antarctic Bottom Water into the Brazil Basin. Journal of Physical Oceanography 23:2667-2682 doi:10.1175/1520-0485(1993)023<2667:tfoabw>2.0.co;2

Stramma L, England M (1999) On the water masses and mean circulation of the South Atlantic Ocean. Journal of Geophysical Research: Oceans 104:20863-20883 doi:10.1029/1999jc900139

Turner J, Overland J (2009) Contrasting climate change in the two polar regions. Polar Research 28:146-164 doi:10.1111/j.1751-8369.2009.00128.x

Vanicek M, Siedler G (2002) Zonal Fluxes in the Deep Water Layers of the Western South Atlantic Ocean. Journal of Physical Oceanography 32:2205-2235 doi:10.1175/1520-0485(2002)032<2205:zfitdw>2.0.co;2

Waterman S, Naveira Garabato AC, Polzin KL (2013) Internal Waves and Turbulence in the Antarctic Circumpolar Current. Journal of Physical Oceanography 43:259-282 doi: 10.1175/JPO-D-11-0194.1

Watson AJ, Ledwell JR, Messias MJ, King BA, Mackay N, Meredith MP, Mills B, Naveira Garabato AC (2013) Rapid cross-density ocean mixing at mid-depths in the Drake Passage measured by tracer release. Nature 501:408-411 doi:10.1038/nature12432

Whitworth T, Nowlin WD (1987) Water masses and currents of the Southern Ocean at the Greenwich Meridian. Journal of Geophysical Research: Oceans 92:6462-6476 doi:10.1029/JC092iC06p06462

Williams A, Bacon S, Cunningham S (2006) Variability of the Lower Circumpolar Deep Water in Drake Passage 1926–2004. Geophysical Research Letters 33:L03603 doi:10.1029/2005gl024226

Zenk W, Hogg N (1996) Warming trend in Antarctic Bottom Water flowing into the Brazil Basin. Deep Sea Research Part I: Oceanographic Research Papers 43:1461-1473 doi:http://dx.doi.org/10.1016/S0967-0637(96)00068-4

Zika JD, Sloyan BM, McDougall TJ (2009) Diagnosing the Southern Ocean Overturning from Tracer Fields. Journal of Physical Oceanography 39:2926-2940 doi:10.1175/2009jpo4052.1

Figure 1 – Produced using Ocean Data View

Practical Salinity on the 28.05 kg/m^3 Neutral Density surface

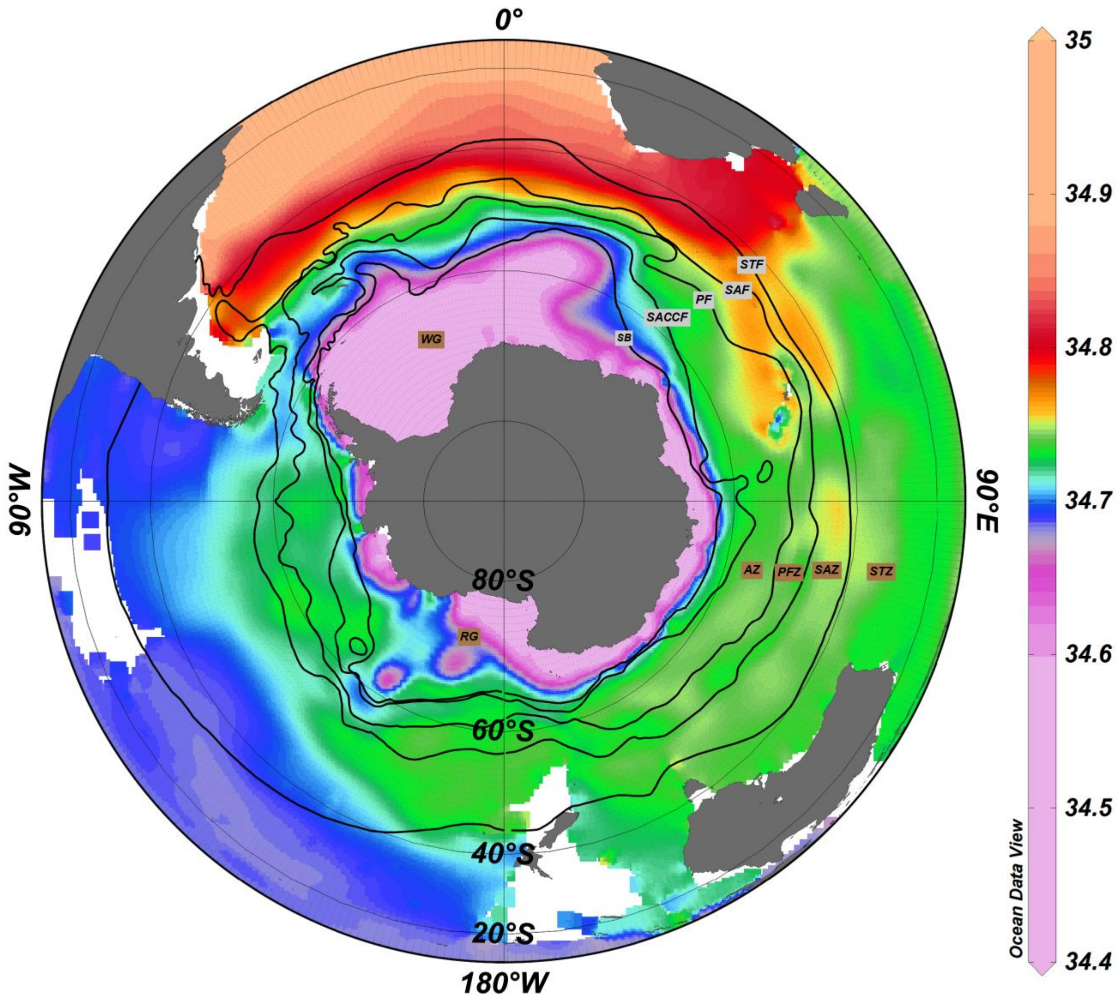

Figure 2 – Produced using Ocean Data View

Major bathymetric features of the Southern Ocean

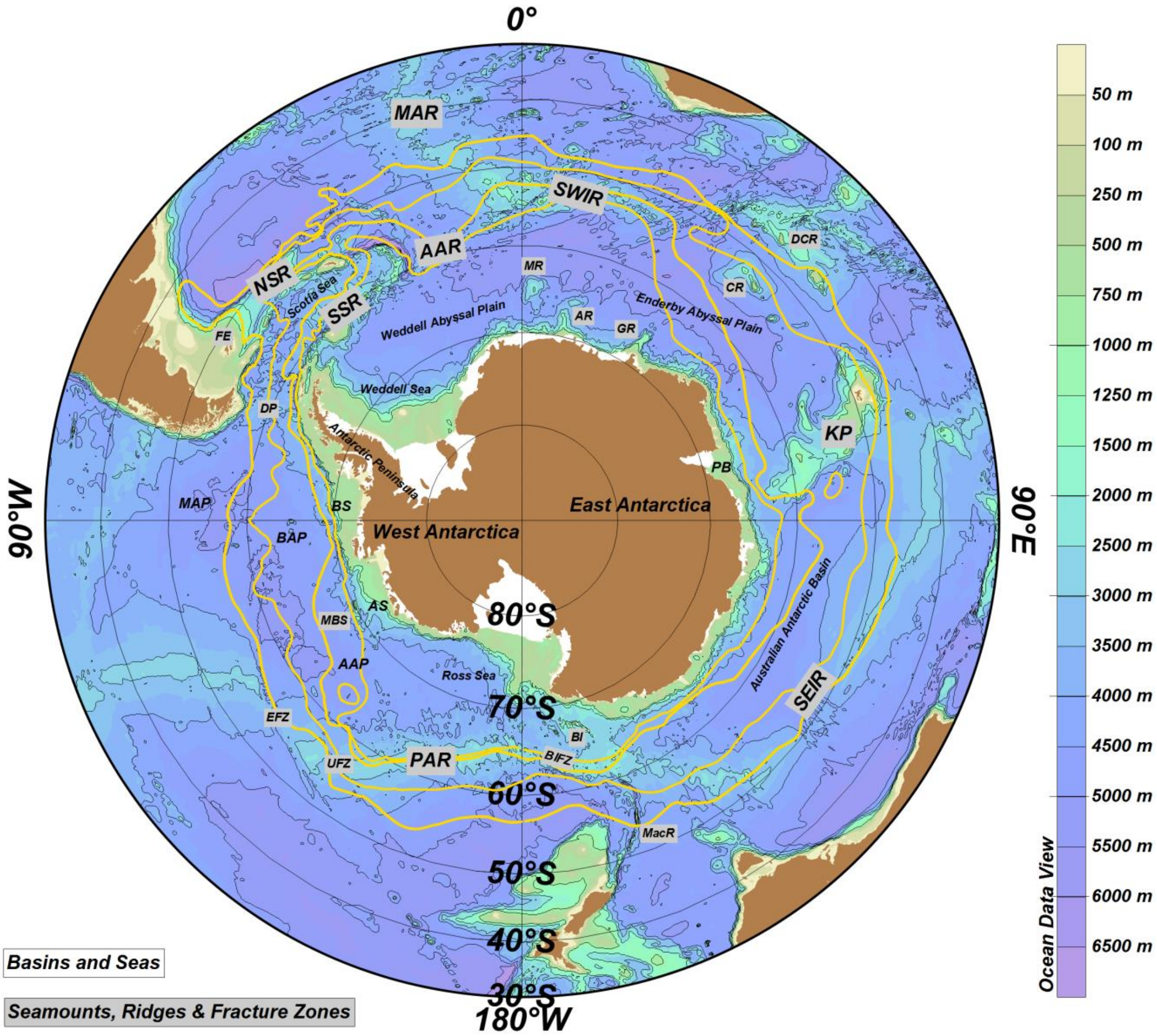

Figure 3 – Produced using Ocean Data View

Location of the hydrographic sections and indicative circumpolar fronts

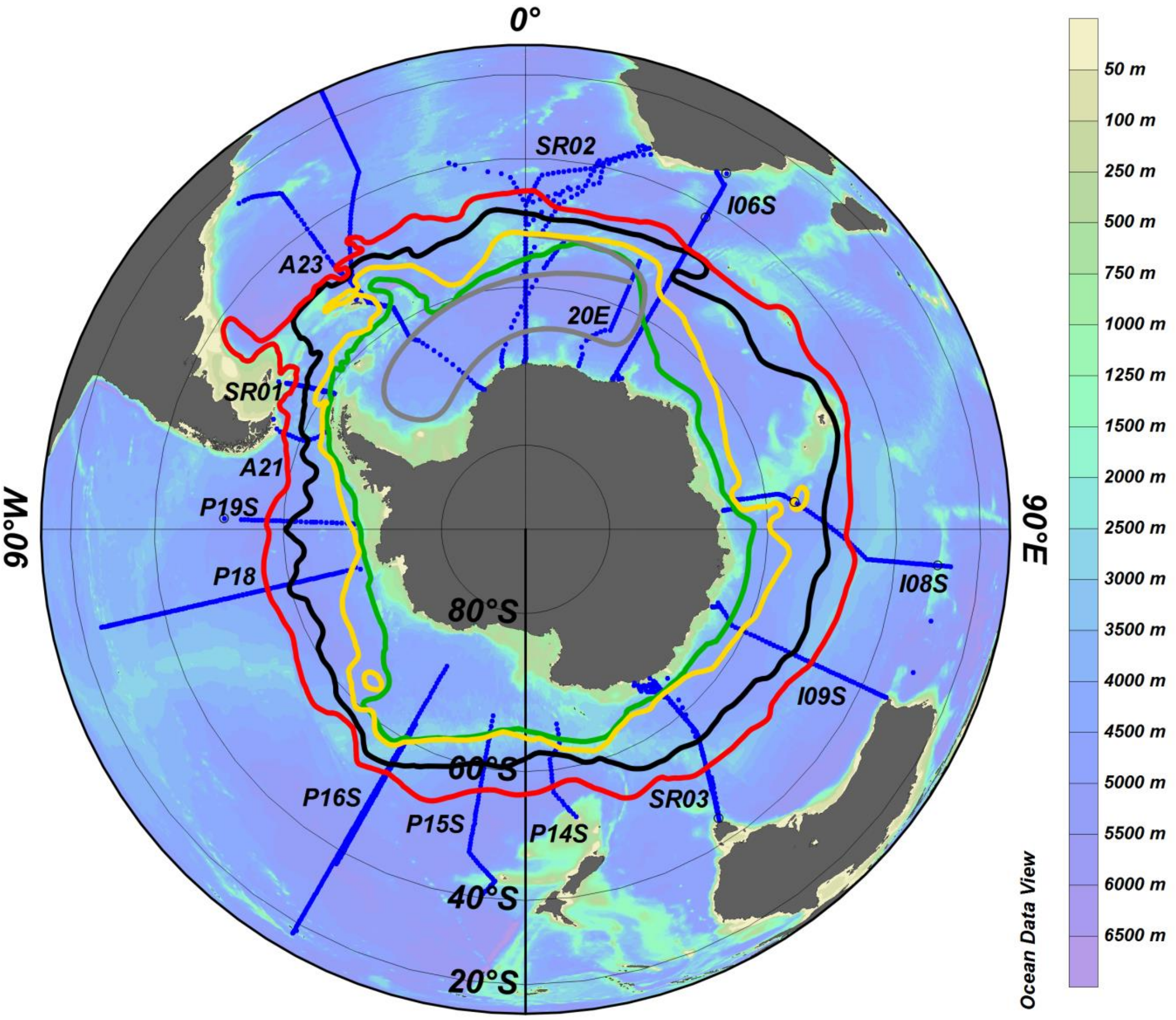

Figure 4 – Produced in Matlab

Potential temperature vs. practical salinity plot for the entire A12-1992 cruise

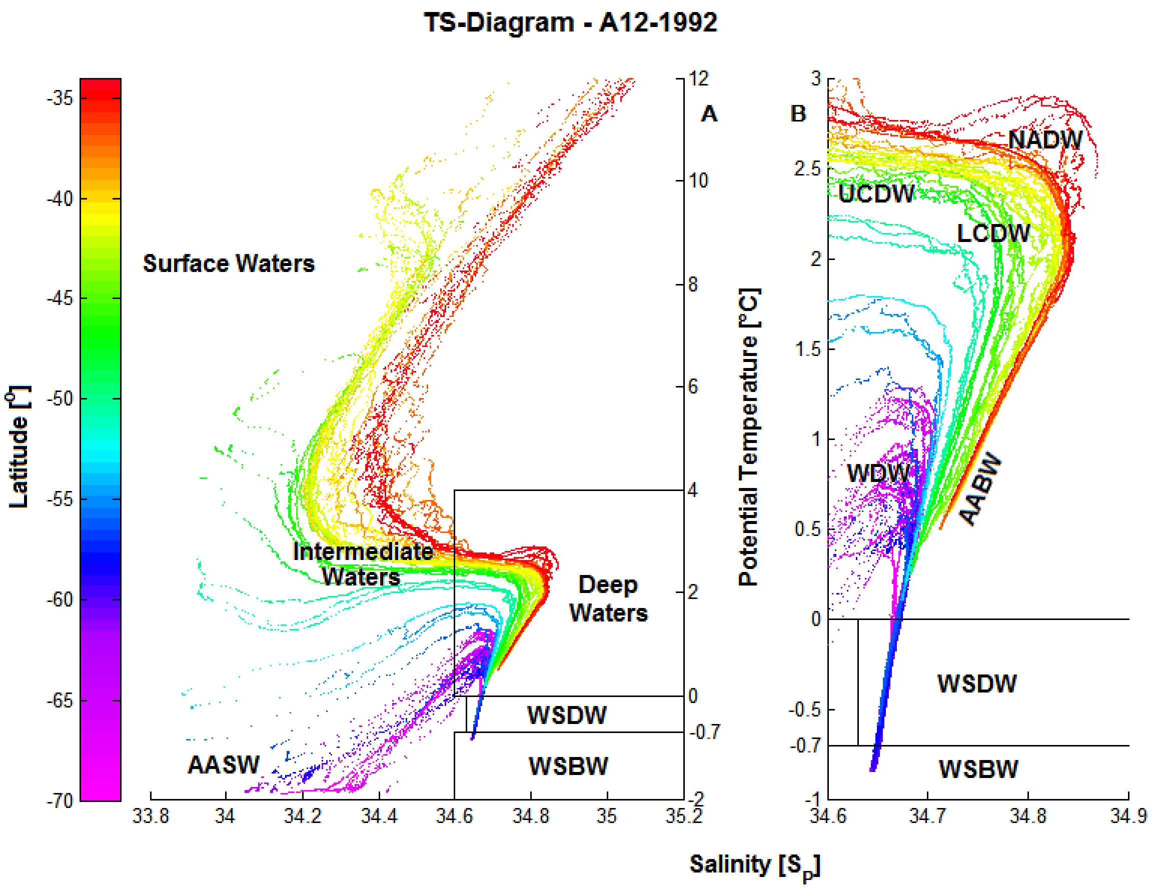

Figure 5 – Produced in Matlab

Variations in the circumpolar salinity-maximum

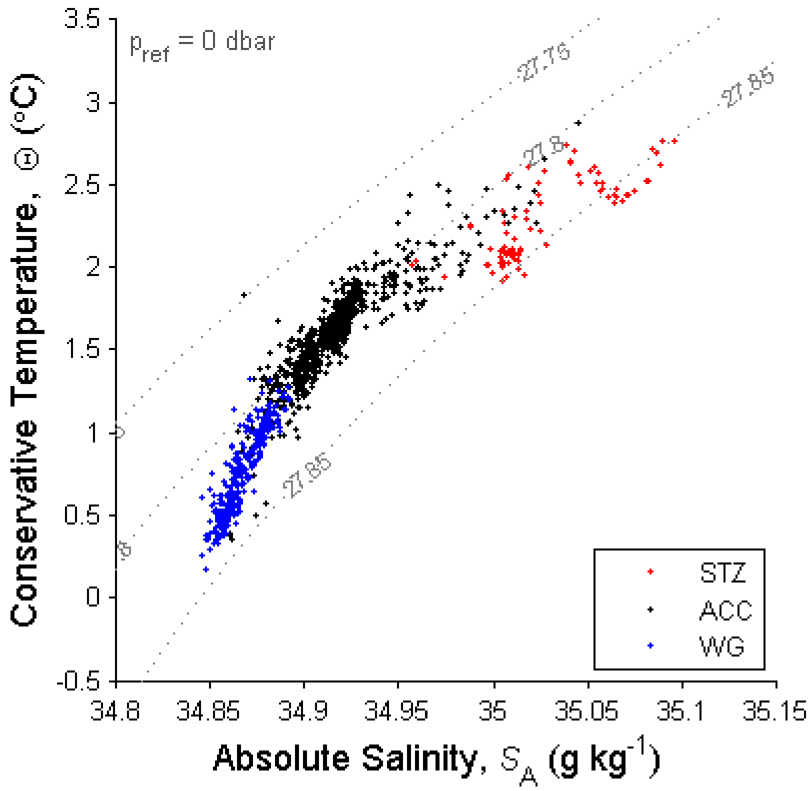

Figure 6 – Produced in Matlab

Salinity maximum variability with potential density and Neutral Density

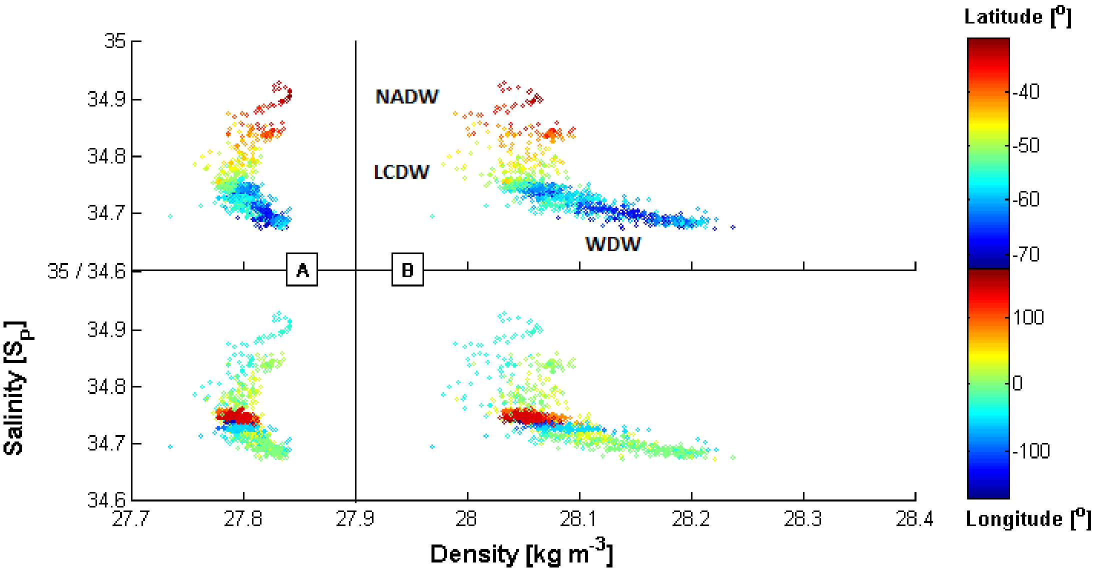

Figure 7 – Produced in Matlab

Salinity maximum values for all stations on all sections plotted against the latitude of the station

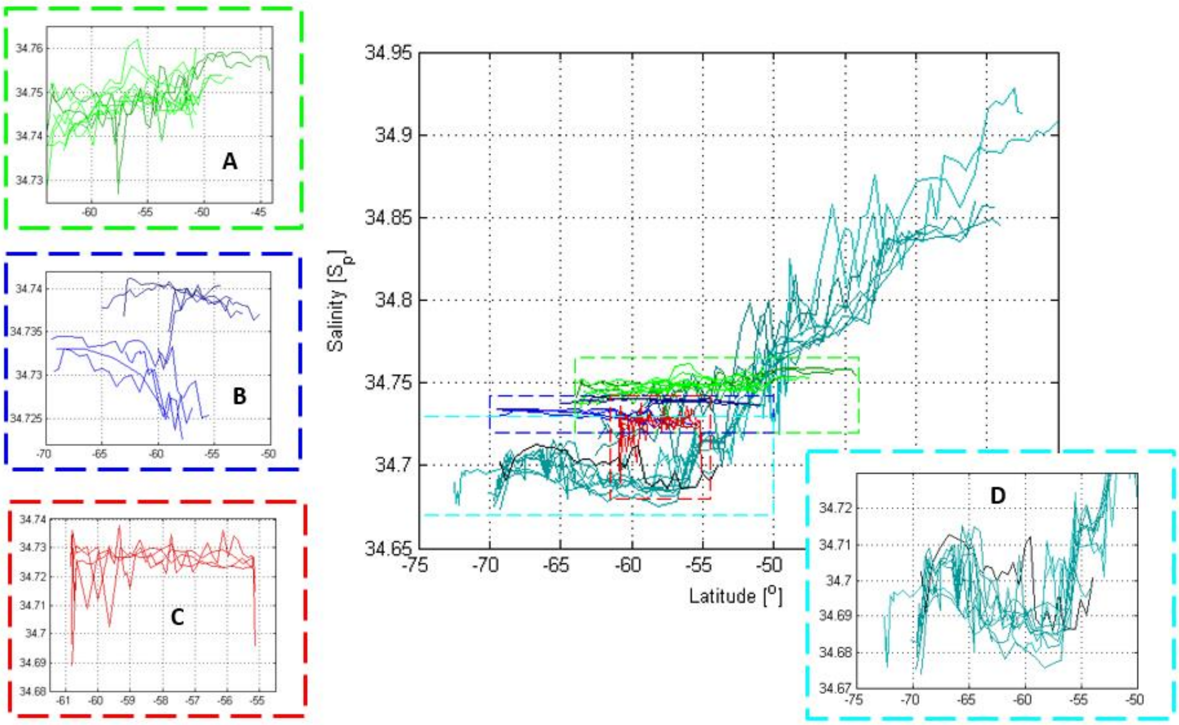

Figure 8a – Produced in Matlab

Spatial change in salinity along the downstream path of the salinity-maximum with regime-based dS/dx linear fits

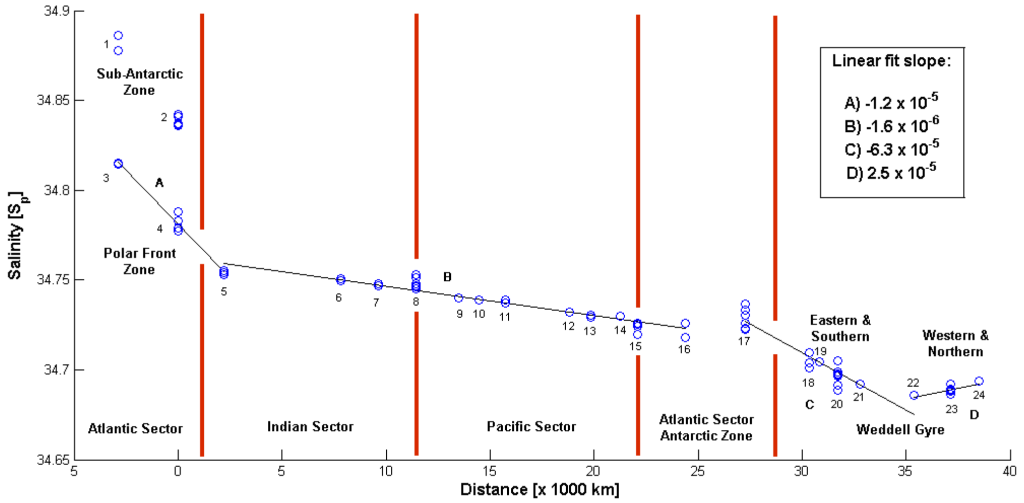

Figure 8b – Produced in Matlab

Spatial change in pressure along the downstream path of the salinity-maximum

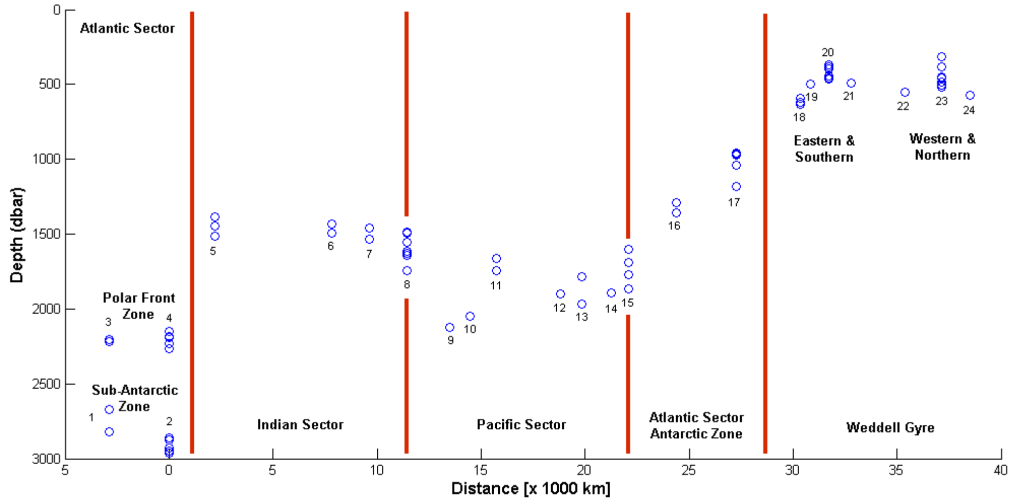

Figure 9 – Produced in Matlab, exported via PDF

Temporal change in the salinity maximum at different sections

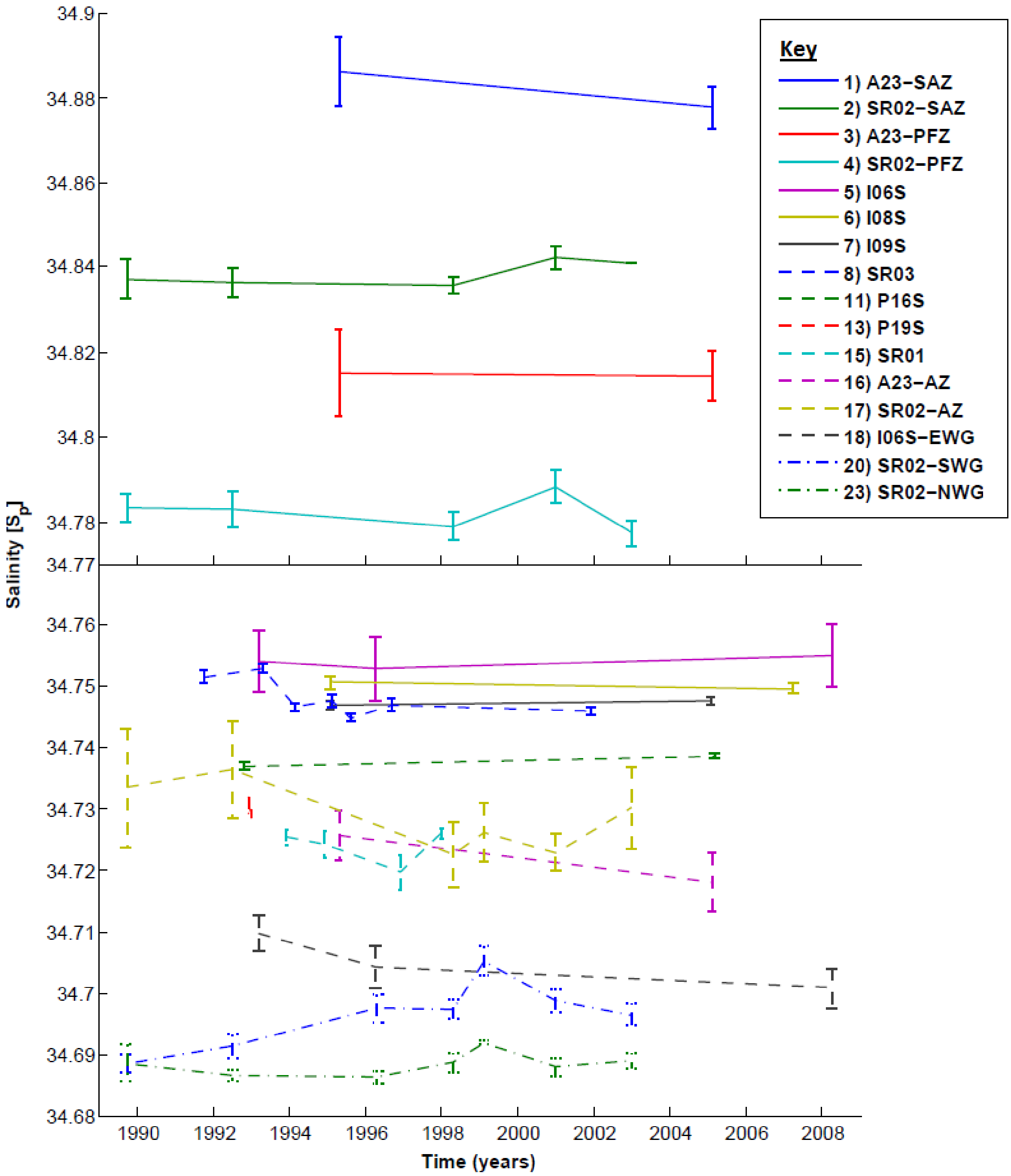

Figure 10 – Ocean Data View combined with grouped shape art in Word

Schematic of propagation of the salinity maximum

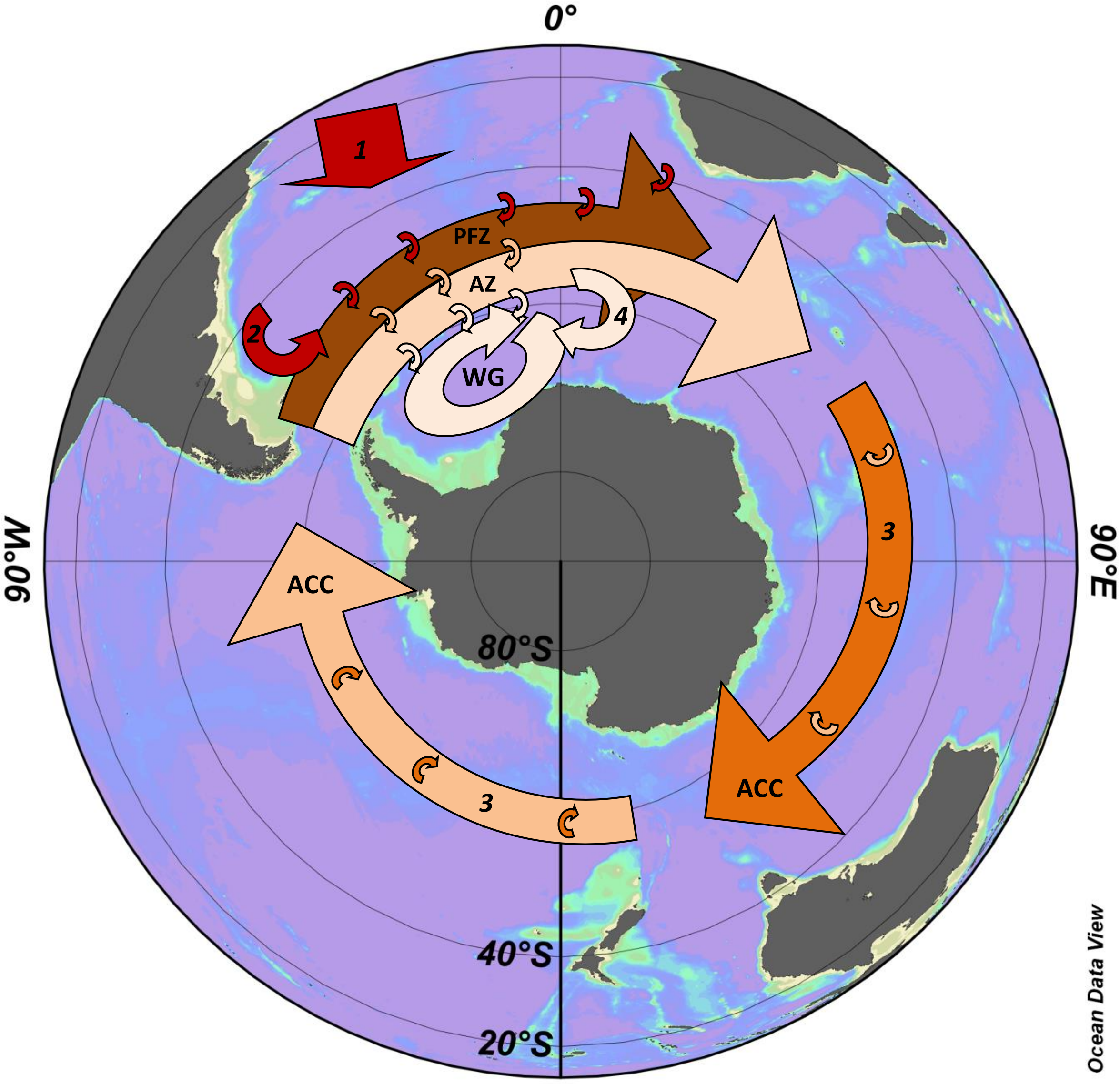

Figure 11 – Produced in Matlab

1-d model results of the modification of practical salinity and Neutral Density

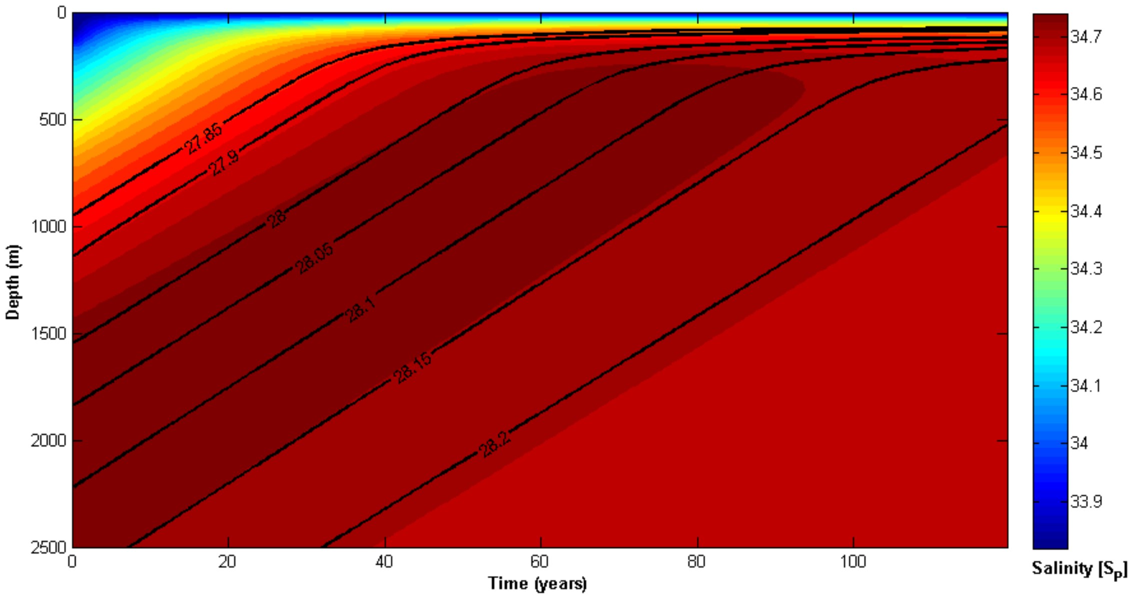

Table 1

Section code (1)	Approx. Longitude (2)	Sub-section no. (3)	Eastward path distance from Greenwich Meridian, including sub-section tags (4)	Cruise ref. Code (5)	No. of stations	EXPO code (6)	Cruise dates (7)
A23	35°W (for ACC)	1 3 16 21 22	-2900 (SAZ) -2900 (PFZ) 24400 (AZ) 32800 (SWG)* 35400 (NWG)*	A23	103	A16S_74JC10_1	20th Mar - 6th May 1995
				A16S-2005*	60	A23_33RO200501	11th Jan - 24th Feb, 2005
SR02	0°	2 4 17 20 23	0 (SAZ) # 0 (PFZ) # 27300 (AZ) ^ 31800 (SWG) * 37100 (NWG) *	SR02 # ^	51	SR02_06MT11_5	6th Sept - 8th Oct, 1989
				SR02-A *	43	SR02_06AQANTVIII_2	6th Sept - 8th Oct, 1989
				A12-1992 # ^*	52	A12_06AQANTX_4	21st May - 5th Aug, 1992
				S04A *	48	S04_06AQANTXIII_4	17th Mar - 20th May, 1996
				SR04-E # ^*	46	SR04_06AQANTXV_4	31st Mar - 21st May, 1998
				A12-1999 ^*	26	A12_06ANTXVI_2	9th Jan, 1999 - 16th Mar, 1999
				A12-2000 # ^*	28	A12_06ANTXVIII_3	11th Dec, 2000 - 11th Jan 2001
				A12-2002 # ^*	11	A12_ANTXX_2	26th Nov, 2002 - 15th Jan, 2003
I06S	30°E	5 18	2200 (ACC) 30300 (EWG)	I06S-A	30	I06SA_35MFCIVA_1	23rd Jan - 9th Mar, 1993
				I06S-B	28	I06SB_35MF103_1	20th Feb - 22nd Mar, 1996
				I06S-2008	27	I06S_33RR20080204	4th Feb - 17th Mar, 2008
I08S	90°E	6	7800	I08S	27	I08S_316N145_5	1st Dec, 1994 - 19th Jan, 1995
				I08S-2007	33	I8S_33RR20070204	4th Feb - 18th Mar, 2007
I09S	115°E	7	9600	I09S	35	I09S_316N145_5	1st Dec, 1994 - 19th Jan, 1995
SR03	141°E	8	11500	SR03-A	20	I09S_09AR20041223	25th Sept - 27th Oct, 1991
				SR03-B	30	SR03_09AR101_1	11th Mar - Apr 03, 1993
				SR03-C	16	PR12_09AR309_1	1st Jan - 1st Mar, 1994
				S03	12	PR12_09AR407_1	13th Dec, 1994 - 2nd Feb, 1995
				SR03-D	28	SR03_09AR9404_1	17th Jul - 2nd Sept, 1995
				SR03-G	5	SR03_09AR9501_1	22nd Aug -22nd Sept, 1996
				SR03-2001	22	SR03_09AR9601_1	29th Oct - 22nd Nov, 2001
P14S	172°E	9	13500	P14S	15	SR03_09AR200011029	5th Jan - 10th Mar, 1996
P15S	170°W	10	14500	P15S	23	P14S_31DSCG96_1	5th Jan - 10th Mar, 1996
P16S	150°W	11	15800	P16A	23	P15S_31DSCG96_1	6th Oct - 25th Nov, 1992
				P16S	23	P16A_316N138_9	9th Jan - 19th Feb, 2005
P18	103°W	12	18800	P18-2008	43	P16S_33RR200501	15th Dec , 2007 - 23rd Feb, 2008
P19S	88°W	13	19900	SR01-B	53	P17E_316N138_10	11th Nov - 17th Dec, 1992
				P19S	75	P18S_31DSCG94_2	4th Dec, 1992 - 22nd Jan 1993
A21	68°W	14	21200	A21	29	P18_33RO20080121	23rd Jan - 8th Mar, 1990
SR01	57°W	15	22100	SR01-E	65	SR01_74DI198_1	20th Nov - 18th Dec, 1993
				SR01-F	18	P19S_316N138_10	13th Nov - 12th Dec, 1994
				SR01-K	66	A21_06MT11_5	15th Nov - 20th Nov 1996
				SR01-M	43	SR01_74JC27_1	27th Dec, 1997 - 7th Jan, 1998
20E	20°E	19 24	30900 (SWG) 38500 (NWG)	A12-20E	32	A12_ANTXX_2	26th Nov, 2002 - 15th Jan, 2003

Table 2

Section no. (refers to table 1)	Name	NADW %	NADW change	AASW %	AASW change	AABW %	AABW change
1	A23-SAZ	100.0%		0.0%		0.0%	
2	A23-PFZ	89.8%	-10.2%	6.1%	6.1%	4.1%	4.1%
3	SR02-SAZ	86.7%		2.1%		11.2%	
4	SR02-PFZ	79.3%	-7.4%	7.2%	5.1%	13.5%	2.3%
5	I06S	68.6%	-10.7%	7.6%	0.4%	23.9%	10.3%
6	I08S	69.9%	1.3%	8.5%	0.9%	21.6%	-2.2%
7	I09S	69.9%	0.0%	8.8%	0.4%	21.3%	-0.3%
8	SR03	70.1%	0.3%	8.9%	0.0%	21.0%	-0.3%
9	P14S	68.8%	-1.3%	9.5%	0.6%	21.7%	0.7%
10	P15S	68.2%	-0.6%	9.5%	0.0%	22.3%	0.6%
11	P16S	66.7%	-1.5%	9.1%	-0.3%	24.1%	1.8%
12	P18	65.2%	-1.5%	9.4%	0.3%	25.4%	1.3%
13	P19S	64.4%	-0.8%	9.5%	0.1%	26.1%	0.7%
14	A21	62.9%	-1.5%	9.0%	-0.4%	28.1%	2.0%
15	SR01	59.9%	-2.9%	8.8%	-0.2%	31.3%	3.2%
16	A23-AZ	60.3%	0.4%	9.1%	0.3%	30.6%	-0.7%
17	SR02-AZ	62.8%	2.5%	9.2%	0.1%	28.0%	-2.6%
18	I06S-EWG	47.5%	-15.3%	7.5%	-1.7%	44.9%	17.0%
19	20E-SWG	47.8%	0.3%	7.7%	0.1%	44.5%	-0.4%
20	SR02-SWG	41.9%	-5.9%	6.9%	-0.8%	51.2%	6.6%
21	A23-SWG	39.2%	-2.7%	6.6%	-0.2%	54.1%	3.0%
22	A23-NWG	32.5%	-6.7%	5.4%	-1.2%	62.1%	7.9%
23	SR02-NWG	36.2%	3.7%	6.2%	0.8%	57.7%	-4.4%
24	20E-NWG	41.3%	5.1%	7.1%	0.9%	51.7%	-6.0%

Table 3

	#	κ_V ($m^2\ s^{-1}$)	κ_I ($m^2\ s^{-1}$)
SR03 and Pacific sector	15	$2.86 \times 10^{-4} \pm 1.06 \times 10^{-4}$	$8.97 \times 10^{2} \pm 1.67 \times 10^{2}$
Eastern and southern Weddell Gyre	12	$2.39 \times 10^{-5} \pm 2.83 \times 10^{-5}$	$2.47 \times 10^{2} \pm 0.63 \times 10^{2}$
All of above combined	27	$2.86 \times 10^{-5} \pm 2.45 \times 10^{-5}$	$2.62 \times 10^{2} \pm 0.46 \times 10^{2}$